University of Alberta
Printing Department

Digitized by the Internet Archive
in 2019 with funding from
University of Alberta Libraries

https://archive.org/details/Tepper1965

Thesis
1965
#81

THE UNIVERSITY OF ALBERTA

A FERRITE MICROWAVE AMPLITUDE MODULATOR

by

BERTHOLD TEPPER

A THESIS
SUBMITTED TO THE FACULTY OF GRADUATE STUDIES
IN PARTIAL FULFILMENT OF THE REQUIREMENTS FOR THE DEGREE
OF MASTER OF SCIENCE

DEPARTMENT OF ELECTRICAL ENGINEERING

EDMONTON, ALBERTA

APRIL 1965

UNIVERSITY OF ALBERTA

FACULTY OF GRADUATE STUDIES

The undersigned certify that they have read, and recommend to the Faculty of Graduate Studies for acceptance, a thesis entitled " A Ferrite Microwave Amplitude Modulator" submitted by Berthold Tepper in partial fulfilment of the requirements for the degree of Master of Science.

ABSTRACT

This thesis describes the design of a ferrite microwave amplitude modulator.

If a plane electromagnetic wave encounters a ferrite medium magnetized in the direction of wave propagation its plane of polarization is rotated as the wave propagates in the medium. This principle, known as Faraday rotation , is used in the present design to vary the power output accepted by a standard rectangular X-band guide located at the end of a section of circular guide containing a ferrite rod.

The design depends largely on experimental methods to obtain the necessary dimensions for the circular guide structure. Several experimental guide structures are built and tested with a view to select the one giving the best overall performance as the prototype for the actual modulator.

The results of these experiments are given together with a complete analysis of the modulator performance.

ACKNOWLEDGEMENTS

The project described in this thesis was carried out in the Department of Electrical Engineering, University of Alberta, under the supervision of Professor W. Sinnema to whom the writer wishes to express his sincere thanks and grateful appreciation for his advice and constant encouragement throughout the entire period of this work.

The writer wishes to acknowledge his indebtedness to the Northern Electric Co. Ltd. for its financial assistance during the entire duration of this work.

Many thanks are due to the following:

Professor R.W.King for many helpful suggestions concerning the mechanical design of the Faraday Rotator and for the actual machining of the device.

Mr. E.A.Buck and his staff for their cooperation in providing the many mechanical parts required for this project.

TABLE OF CONTENTS

		Page
Chapter I	The Properties of Ferrites	1
Chapter II	The Faraday Rotation Effect	3
Chapter III	Design Theory of the Ferrite Microwave Amplitude Modulator	6
3.1	Introduction	6
3.2	The Proposed Waveguide Structure of the Modulator	6
Chapter IV	The Design of the Ferrite Microwave Amplitude Modulator	9
4.1	The Ferrite Element	9
4.2	The Waveguide Structure	12
4.2.1.	The Ferrite to Waveguide Diameter Ratio	12
4.2.2	Broadbanding	13
4.2.3	Length of Waveguide Structure	13
4.2.4	Wall Thickness of the Waveguide	14
4.2.5	The Dimensions of the Ferrite Microwave Amplitude Modulator	14
4.2.5.1	The Length of the Round Guide	14
4.2.5.2	The Inside Diameter of the Round Guide	15
4.2.5.2.1	Introduction	15
4.2.5.2.2	Calculation of the Inside Diameter	18
4.3	The Design of the Driving Coil	25
4.3.1	Distributed Winding Capacitance	25
4.3.2	Capacitance to Ground	26
4.3.3.	Wire Size	26
4.3.4	Calculation of Magnetic Field Strength	27
4.3.5	Sample Calculation of the Modulator Coil	31
4.4	The Design of the Coil Driver	34

		Page
Chapter V	Experimental Investigations	35
5.1	The Faraday Rotator	35
5.1.1	Design, Manufacture, and Performance of the Faraday Rotator	35
5.1.2	Experimental Observations made with the Faraday Rotator	43
5.2	Experimental Analysis of the A- and B-Sections	43
5.2.1	Test Procedures	43
5.2.2	Test Results for the B-Sections	47
5.2.3	Test Results for the A-Sections	52
Chapter VI	The Construction and Performance of the Ferrite Microwave Amplitude Modulator	58
6.1	The Construction of the Modulator	58
6.2	The Performance of the Modulator	59
6.2.1	The Coil Performance	59
6.2.2	The Modulator Performance	62
Chapter VII	Conclusion	79
Bibliography		80

LIST OF TABLES

Table		Page
4-1	Magnetic properties of R-1 and R-4 ferrite material as published by the manufacturer (Indiana General Co.)	9
4-2	Design intent for the A- and B-sections	23
4-3	Calculated results for the A- and B-sections	24
5-1	VSWR measurements for the Faraday rotator at 10° intervals as a function of frequency with probe depth as parameter	41
5-2	VSWR measurements for the B-sections	48
5-3	Dissipative loss measurements for B-section #3 & #4	52
5-4	VSWR as a function of frequency (A-sections)	53
5-5	Current requirement for the first transmission minimum (A-sections)	54
5-6	Maximum attenuation at the first transmission minimum (A-sections)	55
5-7	Dissipative losses (A-sections)	56
5-8	Summary of % ratings for the A-sections	57
5-9	Relative comparison between observed and calculated rotations for the A-sections	57

Table		Page
6-1	Experimental and calculated data of the modulator coil	60
6-2	Comparison between modulator and A-section #6 current requirements for the first transmission minimum	62
6-3	Maximum attenuation obtainable with the modulator and A-section #6	63
6-4	Dissipative losses in the modulator and A-section #6	63

LIST OF FIGURES

Figure		Page
3-1	Proposed modulator structure	7
3-2	The modulator transmission system	7
3-3	Modulation cycle	8
4-1	Attenuation characteristics of synthane absorbing vanes as a function of length	16
4-2	Attenuation characteristics of synthane absorbing vanes as a function of frequency	17
4-3	Pie-wound solenoid	26
4-4	Observed field distribution along the longitudinal axis of a solenoid	27
4-5	Coil with rectangular cross-section and uniform current density	29
4-6	Closest packed wire arrangement	30
4-7	Definition of symbols for Bunet's formula giving the inductance of a multilayer coil	33
4-8	Coil driver circuit	34
5-1	Schematic arrangement of components of the Faraday rotator	35
5-2	The matched load for the Faraday rotator	38
5-3	Rotatable joint	38
5-4	Axial distribution of magnetic field strength for the experimental coil #1	39
5-5	VSWR vs. frequency for a)transition plus termination b) Faraday rotator (omm probe penetration)	40
5-6	VSWR vs. frequency for the Faraday rotator as a function of probe penetration	42
5-7	Rotation vs. coil #1 current for a .25" diameter 2" long ferrite rod in a .800" circular guide	44
5-8	Axial distribution of magnetic field strength for the experimental coil #2	44a

Figure Page

5-9 Test set up for measuring variation in transmission of microwave energy as a function of applied dc magnetic field 46

5-10 Transmission characteristics of B-section #4 vs. applied current 49

5-11 Transmission characteristics of B-section #4 vs. applied current 50

5-12 Variation of energy transmission and VSWR vs. coil #2 current for B-section #1 51

6-1 The completed modulator 58

6-2 Axial distribution of magnetic field strength for the modulator coil 61

6-3 VSWR of modulator and A-section #6 as a function of frequency 65

6-4 Current requirement for the first transmission minimum and maximum attenuation vs. frequency 66

6-5 VSWR and dissipative losses in the modulator as a function of frequency 67

6-6 VSWR of the modulator as a function of coil current 68

6-7 Pulse modulation of the modulator at 8.2 Kmc 69

6-8 Pulse modulation of the modulator at 9 KMC 70

6-9 Pulse modulation of the modulator at 10 KMC 71

6-10 Pulse modulation of the modulator at 11 KMC 72

6-11 Pulse modulation of the modulator at 9 KMC (expanded time scale) 73

6-12 Transmission characteristics of the modulator as a function of applied current (f= 8.2 & 8.6 KMC) 75

6-13 Transmission characteristics of the modulator as a function of applied current (f= 9.2 & 9.6 KMC) 76

6-14 Transmission characteristics of the modulator as a function of applied current (f= 11 & 11.4 KMC) 77

6-15 Static pulse modulation cycle showing hysteresis at 9 KMC 78

CHAPTER I

THE PROPERTIES OF FERRITES

Ferrites are magnetic iron oxide compounds belonging to the newer class of ceramic materials which have been developed for high frequency use. The one particularly outstanding property of ferrites which has accounted for their great success in modern technology is the extremely high dc resistivity which can be over a million times higher than that of the commonly known ferromagnetic materials. For example, ferrites have been prepared whose dc resisitivity ranges from 10 ohm-cm to 10^8 ohm-cm. These resistivities are to be compared to 10×10^{-6} ohm-cm for iron to about 100×10^{-6} ohm-cm for other materials.(1) Ferrites have, therefore, replaced many of the well known ferromagnetic materials in applications requiring low eddy current losses.

This high dc resistivity property also accounts for the entirely new application of ferrite materials at microwave frequencies from which the heretofore known materials are definitely excluded. However, the properties of ferrites at frequencies below the microwave region must be differentiated from those at microwave frequencies. Below the microwave frequencies ferrites are characterized by an extremely high dielectric constant whose magnitude can reach as high as 10^5 (2). Initial permeability is relatively low (1) compared to their ferromagnetic counterparts. Similarly their saturation flux density is low, ranging from 1500 to less than 5000 gauss. This limits their use in applications requiring high current densities. In filter and inductor designs the μQ product plays an important role. The following quotation from Owen's paper (1) illustrates how the

selectivity of a filter is greatly improved by the use of a ferrite core. Quote: "Here, with a volume of 1.5 cubic inches, a Q of 500 is obtained at 100 Kc. The core consists of a manganese zinc ferrite with an intrinsic permeability of 1500. A coil wound on a molybdenum permalloy powder ring and previously used for a similar purpose had more than six time the volume but only one-half the Q."

At microwave frequencies other phenomena and properties become important. A ferrite placed in a dc magnetic field, is characterized by a tensor permeability, which accounts for its non-reciprocal properties. For example, Hogan's four port circulator is a device (3) which is based on the non-reciprocal Faraday rotation effect. Another important property is the ferromagnetic resonance, the ability of the electrons to absorb microwave energy when they are in resonance with the frequency of the incoming field. Other microwave ferrite devices that have been designed are: switches, circulators, variable attenuators, isolators, parametric amplifiers, frequency multipliers, phase shifters and others. This thesis describes the design of a microwave amplitude modulator using a ferrite element. This modulator uses the Faraday rotation effect which is discussed in the following chapter.

CHAPTER II

THE FARADAY ROTATION EFFECT

When a plane electromagnetic wave propagates in an infinite ferrite medium magnetized in the direction of wave propagation, the plane of polarization is rotated. This phenomenon, known as Faraday rotation, is a direct consequence of the tensor permeability of the ferrite medium which is given by (ref.4,p.150)

$$\overleftrightarrow{\mu} = \mu_o \begin{vmatrix} \mu & -jk & 0 \\ jk & \mu & 0 \\ 0 & 0 & 1 \end{vmatrix} \qquad (2-1)$$

for a magnetizing field applied in the z-direction.

where

$$\mu = 1 + \frac{\omega_o \omega_M}{\omega_o^2 - \omega^2} \qquad k = \frac{\omega \omega_M}{\omega_o^2 - \omega^2}$$

$\omega_o = \gamma H_o$ $\quad\gamma$ = gyromagnetic constant, rads/sec.oe.

H_o = internal dc magnetic field, oe.

$\omega_M = 4\pi M_o$, saturation magnetization, gauss

$\omega = 2\pi f$ is the operating frequency, rads.

Maxwell's equations for the above physical system are written as follows

$$\nabla \times \vec{E} = -j\omega \overleftrightarrow{\mu} \cdot \vec{h} \qquad (2-2)$$

$$\nabla \times \vec{h} = j\omega\varepsilon \vec{E} \qquad (2-3)$$

eliminating $\vec{E}$ from equation (2-2) gives

$$\nabla \times \nabla \times \vec{h} = -\nabla^2 \vec{h} + \nabla(\nabla \cdot \vec{h}) = \omega^2 \varepsilon \overleftrightarrow{\mu} \cdot \vec{h} \qquad (2-4)$$

The plane wave solution in cartesian coordinates is $\vec{h} = \vec{h}_o e^{-\Gamma z}$

where $\Gamma = \alpha + j\beta$ is the complex propagation constant. Substituting this solution into equ.(2-4) gives

$$-\Gamma^2 \vec{h}_o\, e^{-\Gamma z} + \hat{z}\,\Gamma^2\, h_{ox}\, e^{-\Gamma z} = \omega^2 \varepsilon\, \overleftrightarrow{\mu} \cdot \vec{h}_o\, e^{-\Gamma z} \tag{2-5}$$

in component form equ.(2-5) becomes

$$-\Gamma^2\, h_{ox} = \omega^2 \varepsilon\, \mu_o\, (\,\mu h_{ox} - jk h_{oy}\,) \tag{2-6}$$

$$-\Gamma^2\, h_{oy} = \omega^2 \varepsilon\, \mu_o\, (jk h_{ox} + \mu h_{oy}\,) \tag{2-7}$$

$$0 = \omega^2 \varepsilon\, \mu_o\, h_{oz} \tag{2-8}$$

Taking the ratio of the two equations (2-6) and (2-7) gives

$$\frac{h_{ox}}{h_{oy}} = \frac{\mu h_{ox} - jk h_{oy}}{jk h_{ox} + \mu h_{oy}} \quad \text{it follows that} \quad h_{ox} = \pm\, j h_{oy} \tag{2-9}$$

This means that the solution consists of two plane circularly polarized waves of opposite sense with propagation constants given by

$$\Gamma_{\pm}^{2} = -\omega^2 \varepsilon\, \mu_o (\,\mu \pm k\,) \tag{2-10}$$

where the + sign refers to the positively polarized wave and the - sign to the negatively polarized wave. $\Gamma = \alpha + j\beta$, assuming μ and k to be real

$$\beta_{+} = \omega\sqrt{\varepsilon \mu_o}\; (\,\mu + k\,)^{\frac{1}{2}} \tag{2-11}$$

$$\beta_{-} = \omega\sqrt{\varepsilon \mu_o}\; (\,\mu - k\,)^{\frac{1}{2}}$$

Any linearly polarized wave can be written as the sum of two circularly polarized waves of opposite direction (5).

Let the electric field of a linearly polarized wave be

$$\vec{E} = \hat{x}\, E_1\, e^{j\omega t} \quad \text{at } z = 0 \tag{2-12}$$

This may be written

$$\vec{E} = \frac{E_1}{2}(\,\hat{x} - j\hat{y}\,)\, e^{j\omega t} + \frac{E_1}{2}(\,\hat{x} + j\hat{y}\,)\, e^{j\omega t} \tag{2-13}$$

$$= \vec{E}_{+} + \vec{E}_{-}$$

where $$\vec{E}_+ = \frac{E_1}{2}(\hat{x} - j\hat{y})\, e^{j\omega t} \qquad (2\text{-}14)$$

$$\vec{E}_- = \frac{E_1}{2}(\hat{x} + j\hat{y})\, e^{j\omega t}$$

At z = d these waves become

$$\vec{E}_+ = \frac{E_1}{2}(\hat{x} - j\hat{y})\, e^{j\omega t}\, e^{-j\beta_+ d} \qquad (2\text{-}15)$$

$$\vec{E}_- = \frac{E_1}{2}(\hat{x} + j\hat{y})\, e^{j\omega t}\, e^{-j\beta_- d}$$

adding these two waves gives

$$\vec{E} = \frac{E_1}{2}(\hat{x})(e^{-j\beta_+ d} + e^{-j\beta_- d})e^{j\omega t} - j\frac{E_1}{2}(\hat{y})(e^{-j\beta_+ d} - e^{-j\beta_- d})e^{j\omega t} \qquad (2\text{-}16)$$

by taking out the factor $e^{-j(\beta_+ + \beta_-)d/2}$ the expression becomes

$$\vec{E} = E_1 e^{-j(\beta_+ + \beta_-)d/2}\, e^{j\omega t}\left[\hat{x}\cos(\beta_+ - \beta_-)d/2 - \hat{y}\sin(\beta_+ - \beta_-)d/2\right] \qquad (2\text{-}17)$$

This is a linearly polarized wave. The plane of polarization makes an angle $\theta = \tan^{-1}\frac{E_y}{E_x} = -\tan^{-1}\tan(\beta_+ - \beta_-)d/2 = (\beta_- - \beta_+)d/2$ with respect to the x axis. Consequently the plane of polarization rotates by an amount $(\beta_- - \beta_+)/2$ per unit distance. Substituting the values for β_+ and β_- given by equ.(2-11) shows the dependance of rotation on the permeability tensor

$$\theta = \tfrac{1}{2}(\omega\sqrt{\varepsilon\mu_0})\left[(\mu - k)^{\frac{1}{2}} - (\mu + k)^{\frac{1}{2}}\right]$$

In the previous discussion of the elements of the permeability tensor the tacit assumption is made that the ferrite is fully saturated magnetically. Since it is intended to operate the ferrite below saturation the question arises whether the tensor formulation is still correct in the form given before. Rado (6) has analysed this problem and has arrived at the following values for the elements μ and k.

$\mu = 1;\ k = -\frac{\gamma 4\pi M}{\omega}$ where ω is the operating frequency and M is the magnetization of the sample.

CHAPTER III

DESIGN THEORY OF THE FERRITE MICROWAVE AMPLITUDE MODULATOR

3.1. Introduction

Amplitude modulation of microwaves is generally accomplished by modulating the reflector voltage of a reflex klystron. This process is,in general, accompanied by simultaneous frequency modulation. Special waveform modulation such as square wave or pulse can be accomplished without incidental frequency modulation if the waveforms are truly square, are not sloping, and the rise time is short. The modulation of frequency multipliers using varactor diodes presents similar problems.

Thus a modulating device operating independently of the signal source is desirable. Such an apparatus is provided by the ferrite microwave amplitude modulator which modulates directly the microwave energy of a signal source.

3.2. The Proposed Waveguide Structure of the Modulator

In chapter 2 the Faraday rotation principle for an infinite ferrite medium was derived. In this section a practical waveguide structure for the modulator is proposed and the Faraday rotation principle is used to explain how this structure can produce amplitude modulation.

A structure possessing the necessary symmetry for propagating two circularly polarized waves is shown in Fig.3-1. This structure consists of a section of circular guide containing a concentrically placed ferrite rod. The space surrounding the ferrite is some dielectric material having a dielectric constant ε_s. Two absorbing vanes are inserted in the horizontal plane on both ends of the rod to complete the structure. The reasons for the dielectric and the absorbing vanes are given in chapter 4. Around the

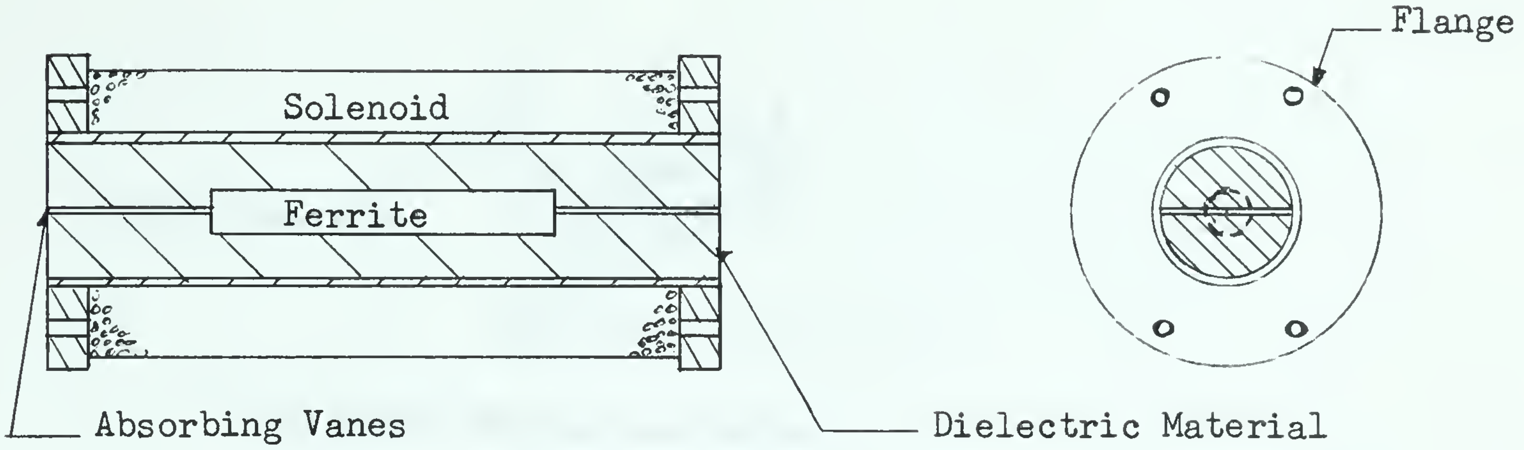

Fig.3-1. Proposed modulator structure.

outside of the circular guide and between the flanges a solenoid is wound providing the dc magnetic field and the time varying signal field. When in use the modulator is placed between two standard rectangular X-band waveguides with the E-field perpendicular to the absorbing vanes as shown in Fig.3-2.

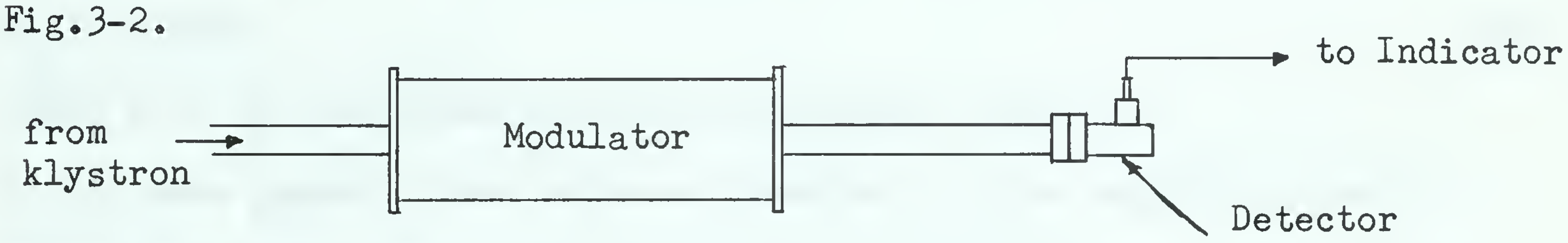

Fig.3-2. The modulator transmission system.

The circular structure permits the propagation of two circularly polarized waves similar to the infinite ferrite medium. As the dc magnetic field is applied these waves propagate with different phase constants and combine after they have passed the ferrite section to form a linearly polarized wave whose plane of polarization has been rotated. The rectangular guide at the output end of the circular section can only receive the vertical component of this wave. This is the basic operating principle of the modulator which is described next in greater detail.

With a certain bias field and signal field applied to the modulator, the output of the crystal, which for the sake of simplicity is assumed to operate linearly, can be described mathematically as follows (see also Fig.3-3).

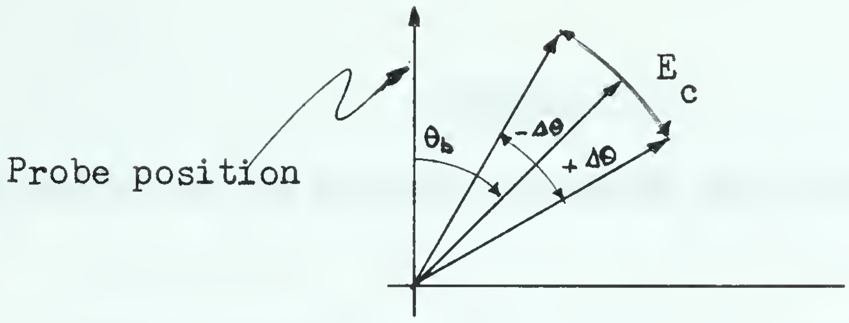

Fig.3-3. Modulation cycle.

Letting the probe output be E_p we get

$$E_p = E_c \cos(\theta_b + \Delta\theta) \qquad (3\text{-}1)$$

where θ_b = the biasing angle

$\Delta\theta$ = the variation in rotation due to the alternating field

E_c = the amplitude of the carrier wave which can be written as

$$E_c = E \sin\Omega t \qquad (3\text{-}2)$$

where E is the amplitude and Ω is the carrier frequency.

In its most general form $\Delta\theta$ is any function of time say $\Delta\theta = \theta_m f(\omega t)$, substituting this expression and equ.(3-2) into equ.(3-1) results in the final form of the field strength at the probe

$$E_p = E \sin\Omega t \cos\left[\theta_b + \theta_m f(\omega t)\right] \qquad (3\text{-}3)$$

If $\theta_b = 0°$ $\quad E_p = E \sin\Omega t \cos\left[\theta_m f(\omega t)\right]$

If $\theta_b = 90°$ $\quad E_p = -E \sin\Omega t \sin\left[\theta_m f(\omega t)\right]$

In the former case E_p can only decrease as the modulating field is applied, in the latter only increase. If it is desired that the rectangular guide is cut-off when no modulating signal is applied, θ_b should equal 90°. Since $\theta_m f(\omega t)$ is usually a pulse signal it is decided to design the modulator for a biasing angle of 90°.

CHAPTER IV

THE DESIGN OF THE FERRITE MICROWAVE AMPLITUDE MODULATOR

There are three main parts that constitute the modulator 1) the ferrite element, 2) the waveguide structure, 3) the coil system. All three items are intimately dependent on each other and very unfortunately, optimizing any one or all of them does not lead to optimum performance of the completed device. The guiding principle used in the design is that of obtaining maximum rotation for reasonable power consumption. A detailed description of each component follows.

4.1. The Ferrite Element

Two ferrite materials were considered for application in the modulator. Their properties are given in Table 4-1.

Table 4-1. Magnetic properties of R-1 and R-4 ferrite material as published by the manufacturer(Indiana General Co.).

Properties	R-1	R-4
μ'/μ_o *	45	40
μ_{max}	320	470
H_c**(oersted)	2.1	1.4
B_r**(gauss)	1240	1490
$4\pi M$ **(gausss)	1760	1780
Minimum Density (gms/cm^3)	4.10	4.15
Curie Temperature (°C)	290	320
Line Width *** (oersted)	490	380
γ **** (1/sec.-oe.)	18.56×10^6	18.12×10^6

* At frequency of 1 Mc/s
** At Hmax = 50 oe.
*** At X-band - 9.430 KMc
**** Measurement made in conformance with proposed ASTM standards

Although the two materials are very much alike, R-4 was chosen for the following reasons:

i) Lowest recommended operating frequency at X-band for R-4 is 7 KMC whereas for R-1 it is only 8.5 KMC. Thus the waveguide structure sets the limit of the bandwidth of the device rather than the ferrite element.

ii) Curie temperature is 320° C for R-4 vs. 290° C for R-1.

iii) The hysteresis loop. It was shown earlier that k, the off-diagonal component of the permeability tensor approximates closely the initial magnetization curve of the ferrite material. Since rotation depends on k and since large differential rotations are desired, the hysteresis loop should rise steeply. R-4 exhibits a steeper rise than R-1, which is also revealed by μ_{max} which is 470 for R-4 and 320 for R-1.

The shape of the ferrite element should be a round rod for reasons of symmetry which will become apparent during the discussion of the waveguide structure. Here again only two choices of standard dimensions existed.

i) type F-703-1 Length = 2" ± .010" , Diameter = .250"± .002"

ii) type F-747-1 Length = 2" ± .010" , Diameter = .125"± .002"

Since the magnitude of the rotation depends strongly on the ferrite to waveguide cross-sectional area, the larger it is the larger the rotation per unit length per unit applied field, type F-703-1 was selected for application in the modulator.

The suitability of the R-4 material was established by two additional considerations a) frequency of operation and state of magnetization of the ferrite, and b) the figure of merit.

a) Frequency of operation and state of magnetization of the ferrite. For maximum differential rotation the ferrite must be operated below magnetic saturation. If, however, the ferrite is not magnetically saturated, so called "low-field" losses can be experienced which can occur at frequencies as high as (ref.4, p.541)

$$(\omega_r)_{max} = \gamma(H_{anis} + 4\pi M) \qquad (4\text{-}1)$$

where $(\omega_r)_{max}$ is the highest frequency at which "low-field" losses can occur, H_{anis} is the anisotropy field, M the state of magnetization. Taking H_{anis} as small (ref.4, p553) equ.(4-1) can be approximated by

$$(\omega_r)_{max} = \gamma 4\pi M_o \qquad (4\text{-}2)$$

Using the properties of R-4 material this works out to

$$(\omega_r)_{max} = (18.12 \times 10^6)(1780)$$

$$f_r = 5.13 \text{ KMC}$$

Since the operating frequency of the modulator is greater than 8 KMC, "low-field" losses are avoided. Thus the magnitude of the saturation magnetization $4\pi M_o$ affects the low frequency limit and the maximum rotation obtainable at saturation.

b) The Figure of Merit. Although perturbation theory is not applicable in the present design since the ferrite waveguide diameter ratio is substantially larger than 0.4, some qualitative estimates can still be obtained by applying a figure of merit derived by perturbation methods. The figure of merit is defined as rotation per unit loss and is given by (ref.4, pp,553-556).

$$F = \omega T$$

where F = figure of merit

T = the relaxation time and is given by $T = \frac{2}{\gamma \Delta H}$

γ = gyromagnetic ratio rads/sec.-oe.

ΔH = line width, oersted

Specifying a maximum attenuation of 0.5 db in the present design and a

maximum rotation of 90° the figure of merit is calculated as follows. The total rotation $\theta_t = \theta \ell = 90°$ in a length ℓ of ferrite. By definition $F = \frac{\theta}{\alpha}$ where α is the dissipative component of the propagation constant. Total attenuation is given by $\alpha \ell = \frac{\theta_t}{F} = \frac{\theta_t}{\omega T}$ and since the total attenuation should not exceed 0.5 db $20 \log \frac{e^{-\alpha \ell}}{e^{o}} = -0.5$ and so $\alpha \ell = 0.0565$. Therefore $\omega T = \frac{\theta_t}{\alpha \ell} = 27.8$.

Using the data of Table 4-1. for R-4 $T = \frac{2}{\gamma \Delta H} = 29 \times 10^{-9}$ sec.

Therefore $F = \omega T = 182 f = 27.8$ where f is in KMC

Hence, the lowest operating frequency for which this figure of merit can still be maintained is f = 153 Mc.

This figure of merit indicates that the modulator should not experience attenuation problems due to low frequency operation.

Summarizing, the ferrite should have a large saturation magnetization and a large figure of merit which is a result of a small line width. The calculations have shown that the selected ferrite material promises satisfactory results.

4.2. The Waveguide Structure

Before determining the inside guide diameter of the structure shown in Figure 3-1, some basic qualitative factors will be pointed out which provide some direction in selecting the best dimensions.

4.2.1. The Ferrite to Waveguide Diameter Ratio

Faraday rotation is directly proportional to the ratio of ferrite diameter to waveguide diameter. Very large ratios would seem advisable in order to obtain large rotations per unit length. However, losses increase and the figure of merit decreases, higher order modes are likely to occur, and matching problems exist due to the high dielectric constant of ferrites ($\varepsilon = 13$).

On the other hand very small values of the ferrite to waveguide diameter ratio cannot be used either, because the rotation per unit length is quite small and impractically long sections are required to achieve the necessary rotations. Therefore, some intermediate value has to be chosen.

4.2.2. Broadbanding

Faraday rotation is frequency sensitive. To compensate for this effect some of the following methods can be applied (ref.4, p.550).

1. Stagger-tuning of Faraday rotators in series
2. Series rotators with bucking frequency dependance
3. Dielectric loading
4. Ridged guides

Dielectric loading was chosen for this project because it is the simplest to apply. It is accomplished by surrounding the ferrite rod with a tube of dielectric which completely fills the space between ferrite and waveguide wall. The price for improved bandwidth is a reduction in rotation and therefore the dielectric constant of the material cannot be too high, lest it competes with the ferrite for the microwave energy. Incidentally, it is surprising that in this case perturbation theory fails completely to predict even qualitatively the behaviour of dielectric loading for large ferrite to waveguide diameter ratios. Perturbation theory states that dielectric loading not only provides greater bandwidth but also increases rotation (ref4.,p.551). However, the numerical values published by R.A. Waldron (7) clearly indicate a decrease in rotation for any increase in the dielectric constant of the material surrounding the ferrite rod.

4.2.3. Length of Waveguide Structure

Rotation is directly proportional to the length of the ferrite rod and to the strength of the applied field. Since large magnetic fields are inconvenient to produce, increasing the ferrite length would seem to be

the best solution. However, since in the presence of the ferrite rod only one of the two circularly polarized wavecomponents experiences the resonance loss phenomenon, increasing the length of the ferrite rod increases the eccentricity of the wave. This makes it impossible to completely isolate the output rectangular guide.

4.2.4. Wall Thickness of the Waveguide (8)

The final waveguide will be surrounded by a solenoid which will carry alternating currents. To these currents the waveguide wall presents a shorted turn in which eddy currents can exist. This causes losses and more power is required to provide the necessary field strength at the ferrite rod. The applied signal field can be visualized as propagating from the inside coil surface toward the ferrite. Therefore, the waveguide wall should be thin enough to provide a low attenuation path for the highest frequency component of the signal and thick enough to prevent radiation losses of the microwave field. At 9 KMC the skin depth in copper is 27.5×10^{-6} in.; three skin depths are usually sufficient to prevent radiation losses. Thus the minimum wall thickness is .000 084 in. To pass a signal pulse of about 5 μsec rise time the system should have an upper 3-db frequency response of $f_2 = 0.35/ t_r$ (ref.9). In the present case this works out to 70 Kc. The skin depth for 70 Kc is .0099 in. Therefore, the maximum wall thickness, taking one third of the previous value, should be about .003 in.

4.2.5. The Dimensions of the Ferrite Microwave Amplitude Modulator

Keeping the aforementioned guiding principles in mind the design of the actual dimensions of the modulator are approached in the following manner.

4.2.5.1. The Length of the Round Guide

The standard length of the ferrite rod is 2". Calculations,

given in the next section, show that a length of 2" provides sufficient rotation. Therefore, the 2" length is accepted without further modifications. Two horizontal absorbing vanes, 1 in. on either side of the rod, increase the total length of the structure to 4 in.

The two horizontal vanes shown in Fig.3-1 serve a dual purpose. First, as the E vector of the microwave field is turned through 90° the rectangular guide at the load end of the ferrite rod is cut off. The resulting large reflections, if not absorbed, would cause the device to exhibit very large, magnetic field dependent, VSWR 's. Furthermore these reflections, if not absorbed, add to the incident field in such a manner as to produce either increased or decreased rotations depending on the operating frequency. This process leads to serious bandwidth limitations of the device. The vanes will also assure that the plane wave is launched in the round guide with the E vector perpendicular.

In order to determine the lengths of the absorbing vanes needed to obtain sufficient attenuation, experiments were conducted using various lengths of synthane in standard X-band guide. The results are given in Fig.4-1 and Fig.4-2. These figures indicate that a length of 1 in. is sufficiently long to provide the necessary attenuation and that this attenuation is reasonably independent of frequency.

4.2.5.2. The Inside Diameter of the Round Guide

4.2.5.2.1. Introduction

The basis for the computing of the inside diameter is found in a paper written by R.A.Waldron (7). This paper solves Maxwell's equations in circular cylindrical coordinates for the case of an infinitely long, round waveguide containing a concentrically placed round ferrite rod partially filling the guide. The emphasis in this work is on deriving and solving the characteristic equation for the respective phase constants

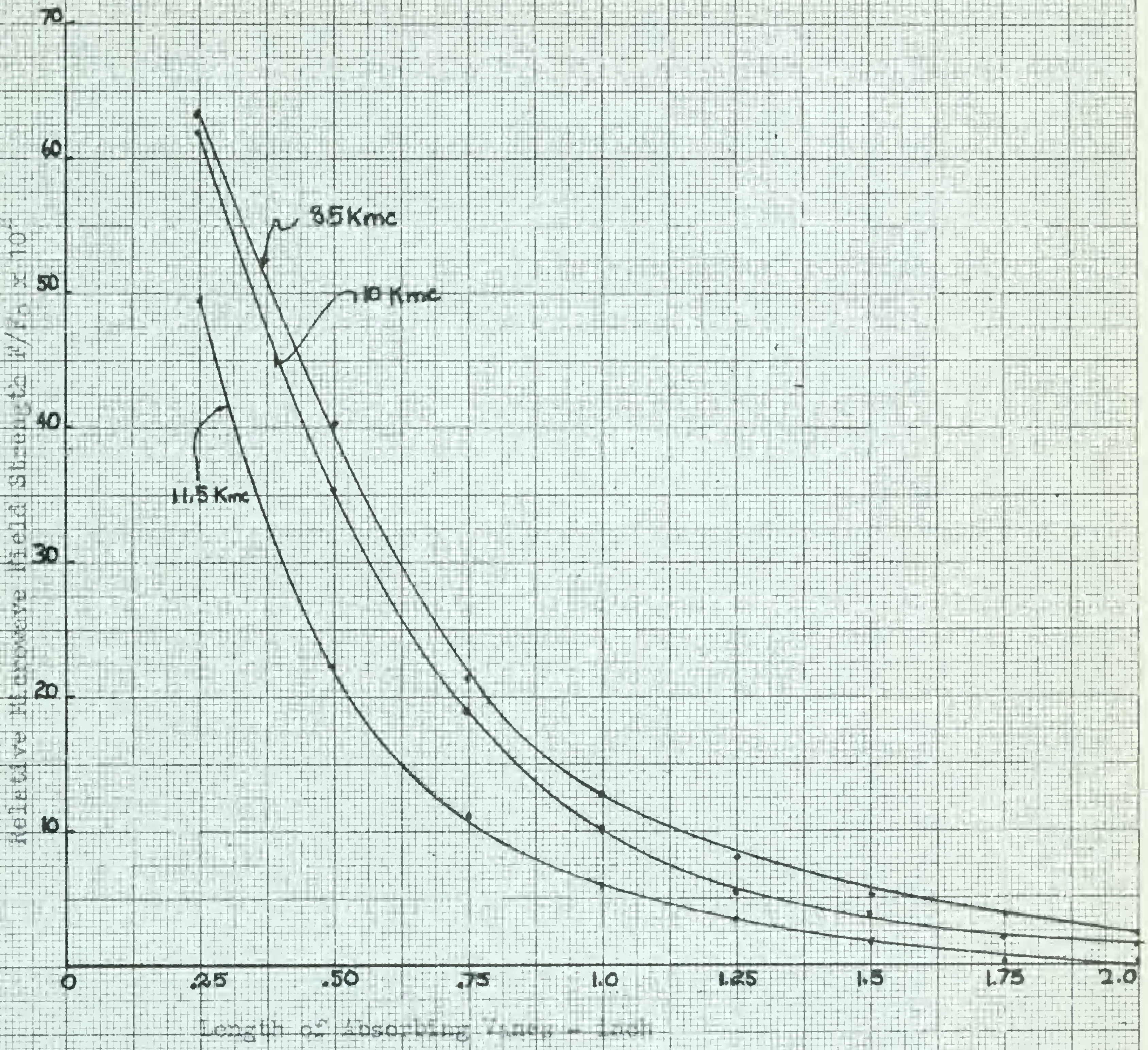

$$\frac{F}{F_0} = \frac{\text{Microwave Field Strength with Vanes}}{\text{Microwave Field Strength without Vanes}}$$

Fig.4-1. Attenuation characteristics of synthane absorption vanes as a function of length.

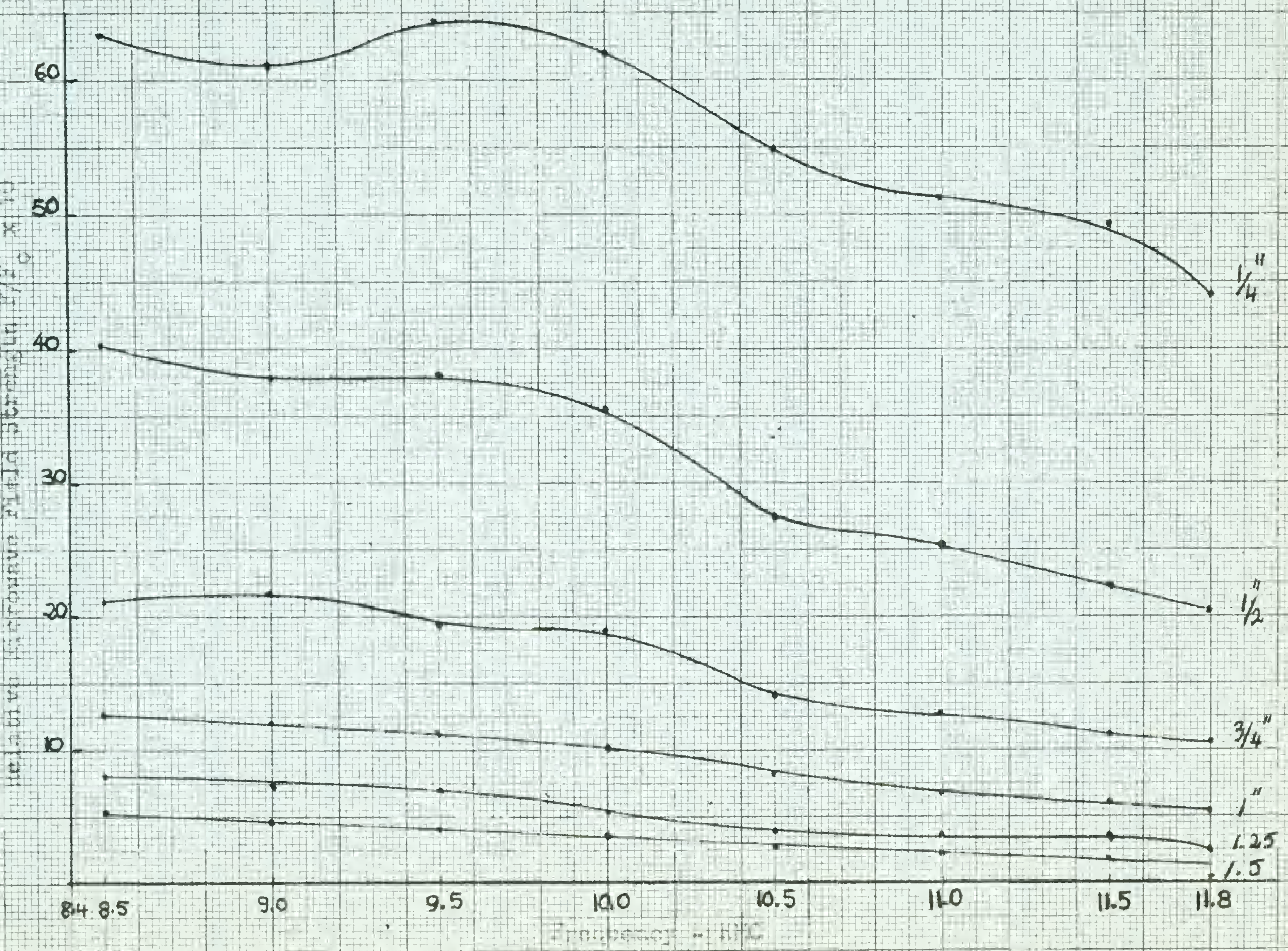

$$\frac{F}{F_0} = \frac{\text{Microwave Field Strength with Vanes}}{\text{Microwave Field Strength without Vanes}}$$

Fig. 4-8. Attenuation characteristics of synthane absorption vanes as a function of frequency.

of the two counter circularly polarized wave components, into which a plane wave will split in the presence of a ferrite rod. The numerical results of this paper are used to calculate the inside diameter of the waveguide. Since Waldron's paper assumes an infinitely long line and the present ferrite length of 5.08 cm is not small compared to a wavelength of 3.33 cm (for an intended operating frequency of 9 KMC), accurate results are not expected. Therefore, several guide diameters are calculated resulting in a number of waveguide sections which are then analysed experimentally.

Another matter not amenable to theoretical calculations is the matching problem. To keep manufacturing procedures as simple as possible it is decided to dispense with elaborate tapered transition guides from rectangular to round guide. Therefore, this phase alone still requires extensive experimental investigation into the possibility of obtaining a reasonable match when butting the rectangular guide directly to the round guide.

Hence, as mentioned above, a number of different waveguide diameters, based on various points of view to be described in the next section, are calculated using the results of Waldron's paper. The object of the experimental work is to test each waveguide section according to VSWR, losses, attenuation and field requirements to obtain 90° rotation.

4.2.5.2.2. Calculation of the Inside Diameter

Waldron's results are presented in terms of the following parameters which will now be defined (7).

Parameter	Definition
b/a	b and a are the radii of the ferrite rod and waveguide respectively;

Parameter	Definition
a/λ_o	λ_o is the wavelength in an infinite extent of the medium surrounding the ferrite
ε	$\varepsilon = \frac{\varepsilon_f}{\varepsilon_s}$ where ε_f and ε_s are the dielectric constants of the ferrite and the medium surrounding the ferrite respectively.
μ, α	are, respectively, the diagonal and off-diagonal components of the relative permeability tensor; these quantities are relative to the properties of the medium surrounding the ferrite.

μ, and α are given by the following equations, which assume that the ferrite operates under lossless condition.

$$\alpha = \frac{p}{\sigma^2 - 1} \qquad \mu = 1 + \frac{\sigma p}{\sigma^2 - 1} = 1 + \sigma\alpha$$

where $p = \frac{\gamma M_s}{\mu_o \omega}$ and $\sigma = \frac{\gamma h}{\omega}$

and μ_o and h are, respectively, the permeability of the medium surrounding the ferrite and the polarizing magnetic field inside the ferrite. Waldron uses M.K.S. units. Since the properties of the R-4 material are published in gaussian units the quantities in the above equations will also be converted to these units. The equations become

$$p = \frac{\gamma 4\pi M_s}{\omega} \qquad \sigma = \frac{\gamma h}{\omega}$$

where γ is in rads/sec-oe. and $4\pi M_s$ is in gauss.

From Table 4-1. $\gamma = 1.812 \times 10^7$ rads/sec.-oe. ; $4\pi M_s = 1780$ gauss

Assuming a frequency of 9 KMC and h about 50 oe., which is the internal field required for saturation α and μ work out to

$p = .571 \qquad \sigma = .016$

thus $\alpha = -.58$ and $\mu = 1 + (.016)(.58) \approx 1$

Unfortunately, Waldron provides numerical values for only the following

values of the design parameters

a/λ_o = .1; .2; .3; .4;
ε = .5; 1.0; 3.0; 5.0; 10.0; 15.0;
α = 0; ± .25; ± .5; ± .75;
μ = .8; 1.0; 1.2;

Therefore, throughout the proceeding calculations $|\alpha|$ will be taken as .5 and μ as 1.0.

For the dielectric sleeve two materials were considered: plexiglass and teflon having dielectric constants of 2.6 and 2.1 respectively. Since $\varepsilon_f = 13.6$, $\varepsilon = \frac{\varepsilon_f}{\varepsilon_s}$ works out to 5.23 for plexiglass and 6.48 for teflon. As 5.23 is sufficiently close to 5.0, that value will be used in the forthcoming calculations for plexiglass; the value of 6.48 is relatively far away from 5.0 to necessitate interpolation between 5 and 10.

Before proceeding with the actual computations Waldron's data were studied from the point of view of establishing trends in the change of ϕ_s, the specific rotation which is defined as the actual rotation per unit length (λ_o being the unit) expressed as a multiple of this unit. ϕ_s is equal to ($\bar{\beta}_+ - \bar{\beta}_-$) where $\bar{\beta}_+$ and $\bar{\beta}_-$ are the phase constants normalized with respect to $1/\lambda_o$ which are obtained from the tables in Waldron's paper. The results of these observations are:

i) ϕ_s increases for increasing ε, which means for decreasing ε_s. This increase is sufficiently linear to justify interpolation.

ii) ϕ_s increases rapidly for increasing values of b/a. The change in ϕ_s due to increasing ε increases for increasing values of b/a.

iii) ϕ_s increases for increasing α, but ε has little effect on these increases, i.e. the increase in ϕ_s from say $|\alpha| = .25$ to $|\alpha| = .5$ is about the same for $\varepsilon = 10$ and $\varepsilon = 15$.

iv) ϕ_s increases with increasing frequency, the increase being most drastic

with increasing $\mathcal{E}$. Note that in the interest of broadbanding ε must be kept low i.e $\mathcal{E}_s$ high.

With these observations in mind one sample calculation is presented to illustrate the method used to obtain the inside guide diameter dimensions of the test sections.

Example

This example applies to the structure that was finally chosen for the prototype of the modulator. As the modulator should operate near 9 KMC the operating frequency is fixed at 1.125 $f_{cut-off}$, where $f_{cut-off}$ is the cut-off frequency for the guide completely filled with the dielectric material.

$f_{operating} = 1.125\, f_{cut-off}$

f_c is chosen at 8 KMC which places f_o at 9 KMC. The dielectric material is chosen to be teflon $\mathcal{E}_s = 2.1$

The cut-off condition for circular guides is $a/\lambda_{oc} = .293$

λ_o at 8 KMC = 2.59 cm for a guide completely filled with teflon. Thus the cut-off wavelength determines the guide dimension which is $a = .758$ cm

Thus $b/a = \frac{(.25)(2.54)}{(2)} \frac{}{(.758)} = .42$

for 9 KMC $\lambda_o = 2.3$ cm $\therefore$ $a/\lambda_o = .33$

Now ϕ_s has to be determined by successive interpolation between $b/a = .4$ and $.45$; $a/\lambda_o = .3$ and $.4$; $\mathcal{E} = 5$ and 10.

First, the interpolation between $b/a = .4$ and $.45$ is carried out keeping a/λ_o and $\mathcal{E}$ constant, then keeping ε constant it is interpolated between $a/\lambda_o = .3$ and $.4$ using the results determined in the previous step; finally having performed the same two steps for $\varepsilon = 10$, interpolation between $\mathcal{E} = 5$ and 10 is performed, during this interpolation $\alpha = \pm .5$ and $\mu = 1$ which is our original assumption for these two values.

$\varepsilon = 5$

$a/\lambda_o = .3$	$a/\lambda_o = .4$
ϕ_s for$(b/a=.4) = .321$ Table 9d(7)	ϕ_s for $(b/a=.4) = .756$ Table 12c(7)
ϕ_s for$(b/a=.45) = .516$	ϕ_s for $(b/a=.45) = .916$
$\therefore \phi_s$ for$(b/a=.42) = .399$	$\therefore \phi_s$ for $(b/a=.42) = .820$

Interpolation between $a/\lambda_o = .3$ and $.4$ results in

ϕ_s for $(a/\lambda_o = .3;\ b/a = .42;\ \varepsilon = 5) = .5253$

$\varepsilon = 10$

$a/\lambda_o = .3$

ϕ_s for $(b/a = .4) = 1.481$ Table 9e(7)

ϕ_s for $(b/a = .45) = 1.67$

ϕ_s for $(b/a = .42) = 1.557$

Waldron gives no values for $a/\lambda_o = .4$, therefore, only the value for $a/\lambda_o = .3$ is used. Finally interpolating between $\varepsilon = 5$ and 10 yields

ϕ_s for $(a/\lambda_o = .33;\ b/a = .42;\ \varepsilon = 6.475) = .829$

Using Waldron's formula $\phi = \frac{180}{\lambda_o}(\bar{\beta}_+ - \bar{\beta}_-) = 64.8$ deg./cm

Thus the total rotation for a two inch length of ferrite $\phi_t = 330$ deg.

Similarly several other guide diameters were calculated. In four cases it was found that no absorbing vanes could be included because those sections of the guide not containing the ferrite rod were cut-off at the frequency for which rotation calculations were made. Therefore, these sections are only 2" long(the length of the ferrite) and are classified as B-sections, the others containing the absorbing vanes are 4" long and are designated as A-sections. Table 4-2 lists the design intent of each section and Table 4-3 gives the results of the computations.

Table 4-2. Design Intent for the A and B Sections

A - Section

Item #	Design Intent
1	Operating frequency is selected at 10 KMC, $\epsilon = 2.6$.
2	Operating frequency is selected at 9 KMC, $\epsilon = 2.6$
3	Same as # 1 , but $\epsilon = 2.1$
4	Operating frequency is selected on the basis of $f_o = 1.125\, f_{cut-off}$. $f_{cut-off}$ is selected at 8 KMC $\epsilon = 2.6$
5	Same as # 2 , except $\epsilon = 2.1$
6	Same as # 4 , except $\epsilon = 2.1$
7	The inside diameter of the guide is chosen so that areas of respective inside transverse cross sections covered by metal flanges are equal.

B - Section

Item #	Design Intent
1	Waldron's maximum rotation criterion is applied, $\epsilon = 2.6$.
2	Same as A-section # 1, except $a/\lambda_o = .2$
3	Same as # 2, except $\epsilon = 2.1$
4	Operating frequency is selected at 9 KMC, $\epsilon = 2.1$, $a/\lambda_o = .2$

Table 4-3. Calculated Results for the A and B Sections

A - Section

Item #	f_c for ε_s KMC	f_o KMC	ε_s	b/a	Φ_t deg.	Guide I.D. in.
1	9.75	10.	2.6	.57	434	.440
2	8.85	9.	2.6	.515	332	.487
3	9.76	10.	2.1	.512	453	.490
4	8.0	9.	2.6	.466	302	.537
5	8.8	9.	2.1	.46	398	.544
6	8.0	9.	2.1	.42	330	.596
7	7.05	8.54	2.1	.37	258	.677

B - Section

Item #	f_c for ε_s KMC	f_o KMC	ε_s	b/a	Φ_t deg.	Guide I.D. in.
1	16.3	11.1	2.6	.95	410	.264
2	14.65	10.	2.6	.855	358	.293
3	14.65	10.	2.1	.768	415	.326
4	13.2	9.	2.1	.692	334	.362

f_c = cut-off frequency for the guide completely filled with the dielectric.

f_o = operating frequency at which Φ_t has been computed

Φ_t = total rotation per section for a saturated ferrite

4.3. The Design of the Driving Coil

The design parameters influencing the performance of a magnetizing coil are quite numerous and although many of them do not lend themselves easily to mathematical analysis, sufficient criteria are available that show how the performance can be expected to vary when one or more parameters are changed. In this section the following properties and design parameters will be discussed:

1.) Distributed winding capacitance
2.) Capacitance to ground
3.) Wire size
4.) Calculation of magnetic field strength
5.) Calculation of the driving coil

4.3.1. Distributed Winding Capacitance

The current response of a coil to an applied voltage waveform depends largely on its inductance and can be significantly altered by the distributed winding capacitance, which determines the self-resonance of the coil. The winding capacitance can be decreased by winding the coil in several sections and connecting them in series (ref.10,p.145). The capacitance is further proportional to (ref.10,p.144)

$$\ell\left(\frac{r_1 + r_2}{r_1 - r_2}\right)$$

where ℓ is the length, and r_1 and r_2 are the outer and inner radii of the coil respectively. Examining this relationship it is apparent that from the point of view of low distributed capacitance ℓ and r_2 should be small and r_1 should be large. As it is required to maintain a magnetic field over two inches (thelength of the ferrite rod) and at the same time desirable to keep ℓ small, the following dimensions were chosen for the coil former:

5 sections @ .44 in.; each separated by 1/16 in. spacers, total length = 2.45 in. Fig.4-3 shows a pie-wound solenoid.

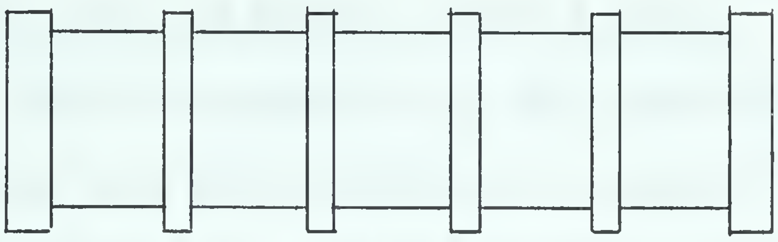

Fig.4-3. Pie-wound solenoid

4.3.2. Capacitance to Ground

The waveguide-coil system can be represented by two concentric metal cylinders, with the waveguide grounded. The capacitance of such a system is proportional to $\left(\ln \frac{r_2}{r_3}\right)^{-1}$, where r_2 is the inside radius of the coil and r_3 the outside radius of the guide. Therefore, making r_2 large would be ideal. This requirement conflicts with the one for low distributed winding capacitance and consequently a compromise has to be made. Also other considerations such as the inductance of the coil, wire length required, construction space available restrict the magnitude of r_2. Thus a separation of .125 in. which forms the thickness of the coil former was chosen. The internal radius of the coil then comes to

.298 in. waveguide radius
.001 in. thickness of metal film
.001 in. clearance
.125 in. thickness of coil former

.425 in. inside radius of the coil

4.3.3. Wire Size

The magnetic field strength is proportional to NI, where N is the total number of turns of wire and I is the current in amperes. The inductance L is proportional to N^2. Thus, decreasing N by a factor of 2 increases I by 2, but decreases L by 4 for the same field strength. Therefore,

the highest current possible should be used. Assuming a maximum current of 100 ma and using the rule of thumb of 1000 circular mils/ amp current carrying capacity establishes wire size # 30 as the wire for the coil.

4.3.4. Calculation of Magnetic Field Strength

After the completion of the experimental work it was found that the final driving coil should provide an average of 26 oe. over the length of the ferrite, i.e. 2 in.. During the design of experimental coils and their subsequent testing it was noted that a uniformly wound cylindrical coil with equal number of turns in each layer has a magnetic distribution along its axis which approximates quite closely an inverted parabola as shown in Fig.4-4. The design formulae available for coils always calculate the field in the centre of the coil where it is a maximum. One obvious approach to compensate for the falling-off of the field distribution is to overwind the ends. This, however, would produce a rather awkwardly shaped coil and as the additive field effect of successive layers of turns diminishes, the overwound ends would become rather bulky. This consideration rendered that approach very unattractive.

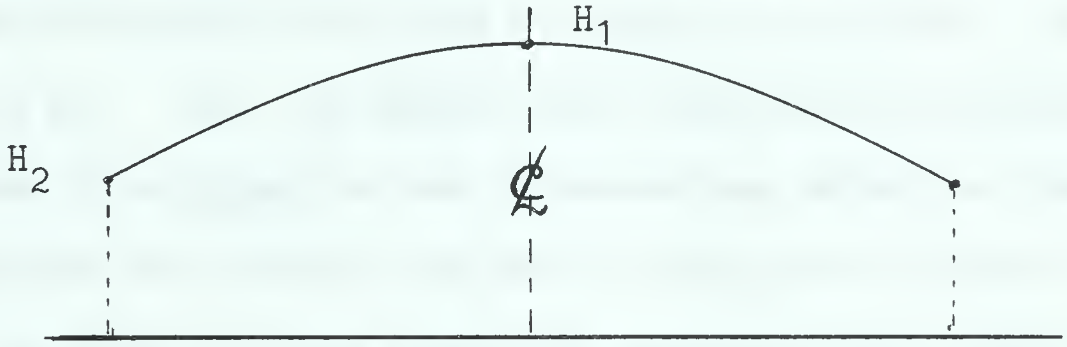

Fig.4-4. Observed field distribution along the longitudinal axis of a solenoid.

The coil shown in Fig. 4-3 has a magnetic field distribution similar to the one shown in Fig.4-4. If the values of H_1 and H_2 are known, the average distribution of magnetic field strength can be estimated by assuming a straight line relationship between H_1 and H_2. This assumption gives an average field distribution of $\frac{H_1 + H_2}{2}$ which is always smaller than the actual distribution. The value of H_1 can be

calculated with good accuracy. However, the value of H_2 is unknown. Since the coil under consideration has five sections, it is suggested to approximate H_2 by the field obtained at the centre of only a single section, since this value can again be calculated by the same methods used for the entire coil of all five sections. It is, of course, realized that the value of H_2 obtained in this manner will always be lower than that as shown in Fig.4-4, since in the actual case the fields of the other sections add to the field of the single end section.

To obtain an approximate relationship between H_1 and H_2 , the field at the centre of a single section, an existing inductance coil consisting of seven indentical sections and being 2.5 in. long, which is close to the length of the coil in Fig.4-3, was tested. It was found that $H_1 = 1.74\ H_2$. With the average field distribution specified, H_2 can be determined by applying the two approximations which have been stated above. An individual coil section can then be designed to provide this field strength (H_2). The value of H_1 can finally be calculated for a coil consisting of five such identical sections.

In the following the method used to calculate H_1 is presented. For cylindrical magnet coils with square ends and uniform current density the magnetic field strength at the centre of the coil is given by (11)

$$H_o = G\sqrt{\frac{\lambda P}{\rho a_1}} \text{ oersted} \qquad (4\text{-}3)$$

where P = ohmic loss power, watts

λ = space factor = $\dfrac{\text{conducting cross-section}}{\text{total cross-section including insulation}}$

ρ = resistivity of the coil conductor, ohm-cm

a_1 = inside radius of the coil, cm

G is a dimensionless factor, the so called Fabry factor and is given by the following expression

$$G = \sqrt{\frac{\pi a_1}{25}}\ \frac{\int_{a_1}^{a_2} \lambda^{+} \iota^{+} \frac{z}{s}\, dr}{\sqrt{\int_{a_1}^{a_2} \varrho^{+} \lambda^{+} (\iota^{+})^{2} rz\, dr}} \qquad (4\text{-}4)$$

where $2z$ = length of current sheet, in the present case equal to the length of the coil

s = is defined by Fig.4-5

ι = current density, amp/cm^2, and the subscript 1 refers to the value of the first layer.

$$\iota^{+} = \frac{\iota}{\iota_1}\ ;\ \lambda^{+} = \frac{\lambda}{\lambda_1}\ ;\ \varrho^{+} = \frac{\varrho}{\varrho_1}$$

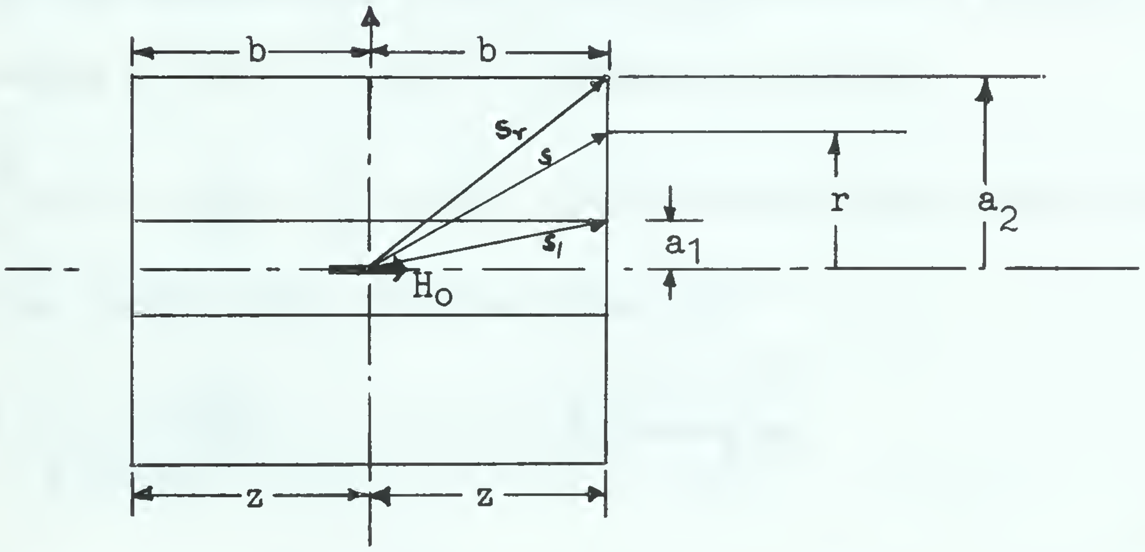

Fig.4-5. Coil with rectangular cross section and uniform current density.

ι^{+}, λ^{+}, ϱ^{+} are considered functions of r, the radial direction of the coil. These given formulae have now to be applied to the present design. Since ι; λ ; ϱ are considered to be independent of r and equal to the value of the first layer, ι^{+}, λ^{+}, ϱ^{+} reduce to the value 1. Also since the coil has square ends, z is a constant and is equal to b, the ½ length of the coil. With these simplifications G becomes

$$G = \sqrt{\frac{\pi a_1}{25}}\ \frac{\int_{a_1}^{a_2} \frac{z}{s}\, dr}{\sqrt{\int_{a_1}^{a_2} rz\, dr}} \qquad (4\text{-}5)$$

s is a function of r and is equal to $s = \sqrt{r^2 + z^2}$ (4-6)

substituting equ.(4-6) into equ.(4-5) gives

$$G = \sqrt{\frac{\pi a_1}{25}} \; \frac{\displaystyle\int_{a_1}^{a_2} \frac{z}{\sqrt{r^2 + z^2}}\, dr}{\sqrt{\displaystyle\int_{a_1}^{a_2} rz\, dr}} \tag{4-7}$$

Evaluating the integrals gives

$$G = \sqrt{\frac{\pi a_1 z}{25}} \; \frac{\ln \dfrac{a_2 + \sqrt{a_2^2 + z^2}}{a_1 + \sqrt{a_1^2 + z^2}}}{\sqrt{\frac{1}{2}\left(a_2^2 - a_1^2 \right)}} \tag{4-8}$$

Now the quantities a_2 and z are normalized with respect to a_1, the inside radius of the coil and are defined as follows

$\frac{a_2}{a_1} = \alpha$; $\frac{z}{a_1} = \frac{b}{a_1} = \beta$ introducing these normalized factors into equ. (4-8) yields G in its final form

$$G = \sqrt{\frac{2\pi\beta}{(25)(\alpha^2 - 1)}} \; \ln \frac{\alpha + \sqrt{\alpha^2 + \beta^2}}{1 + \sqrt{1 + \beta^2}} \tag{4-9}$$

The parameter λ requires some further comments. The factors affecting the winding density are i) roundness of the wire, ii) wire insulation, iii) winding space factor. Since the cross section of the wire is circular the closest packed structure consists of one central wire surrounded by six others as shown in Fig.4-6.

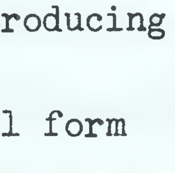

Fig.4-6. Closest packed wire arrangement

If r is the radius of one wire the space factor of this arrangement is given by

$$\lambda_t = \frac{7\pi r^2}{(\pi)(3r)^2} = \frac{7}{9} = .778 \qquad (4\text{-}10)$$

Due to the insulation of the wires the entire cross section is not copper. Hence the space factor correction due to insulation is

$$\lambda_{in} = \left(\frac{d_b}{d_{in}}\right)^2 \qquad (4\text{-}11)$$

where d_b and d_{in} are, respectively, the bare diameter and insulated diameter of the wire. The winding space factor λ_s signifies the practical limitation of attaining λ_t and is usually given by wire tables. Thus the overall space factor becomes

$$\lambda = (\lambda_t)(\lambda_{in})(\lambda_s) \qquad (4\text{-}12)$$

For a coil consisting of several sections an additional space factor correction has to be applied due to the spacing of the sections. If ℓ is the length of the entire coil with spacers and h is its height and w the width of one spacer, the space factor correction λ_c is given by

$$\lambda_c = \frac{\text{area without spacers}}{\text{area with spacers}} = \frac{(\ell - 4w)\ h}{\ell h} = \frac{\ell - 4w}{\ell} \qquad (4\text{-}13)$$

4.3.5. Sample Calculation of the Modulator Coil

Having provided the foundation of the coil design, these principles are now applied to the design of the driving coil of the modulator.

Coil Specifications

Average field intensity H = 26 oe. (see Sect. 5.2.2.)

Inside diameter of coil = .95 in.

Width of spacers = 1/16 in.

Width of pie section = .44 in.

No. of sections = 5

Wire Data for #30 HF

Outside diameter = d_{in} = .0116 in.

Outside diameter of bare wire = d_b = .0100 in.

Winding space factor = λ_s = .89

Resistance per 1000 ft. = R = 104 ohms

In the previous section the assumption was stated that $H_1 = 1.74\ H_2$, and that the average field is given by $\frac{H_1 + H_2}{2}$. Applying these to the present problem results in about 19 oersted as the required field strength of one single section of the coil.

The formulae developed in the previous section require the coil dimensions to be known before H_1 can be calculated. After two trials it was found that N= 400 turns provided the required field strength. This value for N is used in the sample calculation.

From the wire tables these items are calculated :

no. of turns/ in. = $\frac{1}{d_{in}}\ \lambda_s = 76.75 \approx 76$ turns/ in.

$$\lambda_{in} = \left(\frac{d_b}{d_{in}}\right)^2 = .742$$

no. of turns per section is 400; no. of turns/ layer = (76)(.44) = 33

height of coil = $\frac{\text{no. of turns/section}}{\text{no. of turns/ layer}}$(height of one layer) = .14 in.

$$\alpha = \frac{a_2}{a_1} = \frac{.565}{.425} = 1.33 \qquad \beta = \frac{L/2}{a_1} = \frac{.44}{(2)(.425)} = .518$$

Substituting these values into equ.(4-9) yields G = .107 .

The dc resistance of the coil is $R = \frac{(2\pi)(r_m)(R_{1000})(N)}{(12)(1000)}$

where r_m = mean radius of the coil, in.

R_{1000} = resistance of 1000 ft. of wire

N = total no. of turns

On substitution of the appropriate values $R = 10.78$ ohms

Thus the power dissipated $P = I^2R = .1078$ watts, assuming $I = 100$ ma.

$\lambda = (\lambda_t)(\lambda_{in})(\lambda_s) = .514$ substituting these values into equ.(4-3), the magnetic field strength at the centre of a single section becomes

$$H = .107\sqrt{\frac{(.1078)(.514)}{(1.724 \times 10^{-6})(2.54)(.425)}} = 18.45 \text{ oe.}$$

This is sufficiently close to the required value of 19 oe. for H_2 .

The same calculations are repeated for the entire coil consisting of 5 similar sections.

length of coil = $(5)(.44) + 4 \times 1/16 = 2.45$ in.

$$\lambda_c = \frac{\ell - 4w}{\ell} = \frac{2.20}{2.45} = .899$$

$\alpha = 1.33$; $\beta = \frac{2.45}{(2)(.425)} = .2.88$; $G = .103$; $P = (5)(.1078) = .539$ watts

$\lambda = (.514)(.899) = .4625$ thus, $H = 36.6$ oe.

$\frac{H_1 + H_2}{2} = 27.53$ oe. this average is quite satisfactory and is accepted.

The last item of interest is the inductance of the coil which is calculated using Bunet's formula (12)

$$L = \frac{a^2 N^2}{9a + 10\ell + 8.4c + 3.2c\,\ell/a} \ \mu h$$

where the various symbols are defined by Fig. 4-7 .

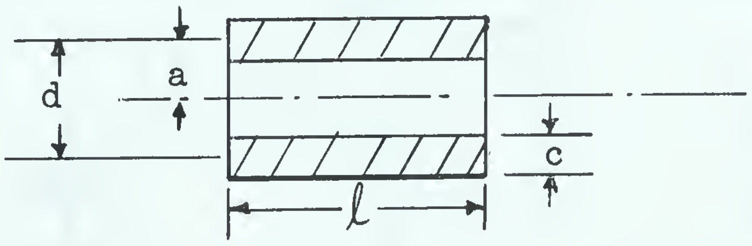

Fig. 4-7. Definition of symbols for Bunet's formula giving the inductance for a multilayer coil.

Substituting in the appropriate parameters the inductance is calculated to be $L = 30.2$ mh .

4.4 The Design of the Coil Driver

In general two separate coils are probably needed to generate the biasing and signal fields. For pulse modulation, however, one coil should be adequate, since a vacuum tube can provide the required pulse modulated coil current.

The inductance of the air cored coil was previously calculated to be 30.2 mh. Inserting the ferrite rod increases the inductance to 58 mh (measured). Therefore, to obtain current pulses through the coil with a rise time of less than 5 µsec. a driver with constant current source characteristics is needed. When determining the wire size to be used as #30, the maximum current requirement was set at 100 ma. To obtain an approximate constant current source being able of supplying 100 ma the 807 pentode was selected. Since according to the manufacturer's specification its plate resistance is in the order of 30,000 ohms, the time constant of the circuit is

$$\tau = L/R = \frac{58 \times 10^{-3}}{30,000} = 1.93 \ \mu\text{sec.} \ ; \text{ the rise time } t_r = 2.2\,\tau = 4.2 \ \mu\text{sec.}$$

This is within the specified rise time limit.

The tube and its associated circuit is shown in Fig. 4-8. A 10 ohm resistor is included in the plate circuit to monitor the current waveform.

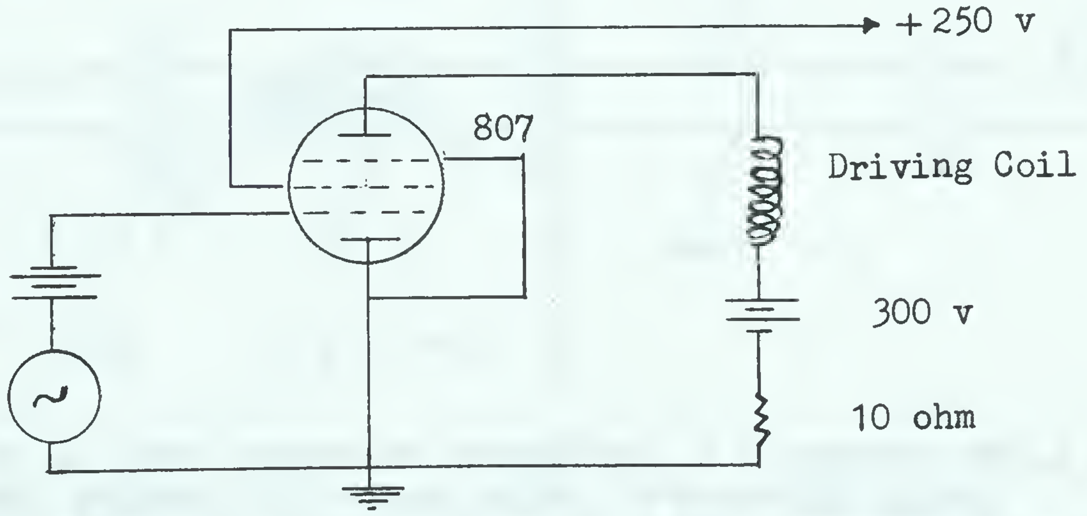

Fig. 4-8. Coil driver circuit.

CHAPTER V

EXPERIMENTAL INVESTIGATIONS

5.1. The Faraday Rotator

To get aquainted with the phenomenon of Faraday rotation and to observe the capabilities of the R-4 ferrite material it was deemed best to start with a waveguide structure that could measure degrees of rotation versus applied dc magnetic field. This device will be termed a Faraday rotator in the following which will describe its design and the results obtained with it.

5.1.1. Design, Manufacture, and Performance of the Faraday Rotator

Fig.5-1 shows a schematic arrangement of those parts that constitute the entire device.

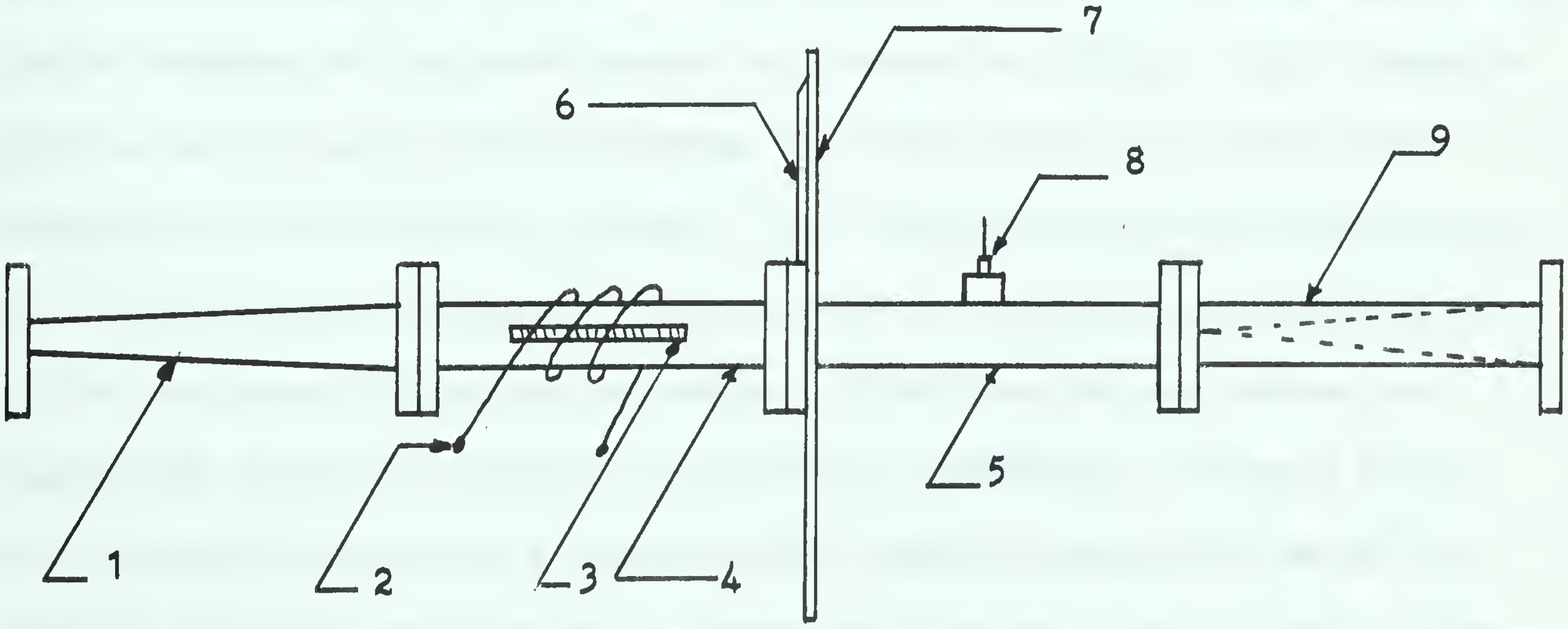

1=rectangular to round waveguide transition, 2 = magnetic field coil
3=ferrite rod, 4=0.800 I.D. round guide, 5= rotatable guide,
6= stationary indicator, 7=protractor, 8= probe, 9= matched load

Fig.5-1 Schematic arrangement of components of the Faraday rotator.

The device operates as follows. Microwave energy is channeled from standard X-band rectangular guide via a rectangular to round waveguide-transition to a 6 in. length of .800 in. inside diameter round guide containing a concentrically placed round ferrite rod. Around this section is wound the dc magnetic field coil. Following this section comes a rotatable round section to which the protractor is attached and which is terminated by a matched load. The rotatable section also contains the probe.

The probe originally, i.e. with zero dc field, receives the maximum field at 0 deg. (deg. are measured from the vertical). As the magnetic field is applied, the plane of polarization is rotated such that the maximum pick up is at some angle θ . Since the probe is mounted in a rotatable waveguide section, it can be rotated until a maximum indication is again obtained. The angle θ is determined from the protractor reading.

The transition piece was designed first. Its length is 6 in. which represents about 4.5 wavelength at 9 Kmc. Therefore, a fairly good match was expected (13) since the transition is several wavelengths long. The inside diameter of the round section was chosen as .800 in. This dimension gives a fairly high cut-off frequency (8.67 KMC) but still permits wave propagation with no ferrite present. The transition piece was manufactured by electroforming techniques. A round mandrel out of wax was machined and cut to the proper dimensions and shape. After this the wax surface was coated with graphite to make it electrically conducting. The work piece was then electroplated in a copper sulfate bath at about 20-40 ma/in^2 of surface area which resulted in a copper built up of 0.010 in./day. After the plating was finished the wax was melted out and the flanges were put on.

An exellent broadband matched load was obtained with a $7\frac{3}{4}$ in. long round waveguide section containing a $7\frac{3}{4}$ in. long continuously tapered rod made of yellow cedar. To enhance the absorption eight synthane absorbing vanes

are placed symmetrically about the longitudinal axis of the rod. The guide is then closed off at the load end by a metal plate. The device is depicted in Fig. 5-2.

The rotatable joint is shown in Fig. 5-3. The rotatable guide is placed into a closely machined recess in the stationary guide. This recess assures that the two guides remain concentric when being rotated. The locking ring fits over the rotatable guide and presses the two movable faces together by means of screws fitting through the locking ring and into the flange of the stationary guide. The locking pressure can be adjusted to suit requirements.

The magnetic coil was designed using the principles of section 4.3.4.. Since it was intended to operate the coil from an existing 24 v dc battery supply, the coil was wound in two sections each having a resistance of 9 ohms. The two sections are then connected in parallel. The data for the finished coil are

wire used # 16

1st coil section 2810 turns, 2nd coil section 1445 turns,

R_{dc} of coil sections connected in parallel = 4.7 ohms

The magnetic field distribution along the axis of the coil as a function of dc current is given graphically by Fig. 5-4..

After all components had been obtained the performance of the rotator was tested. Emphasis was placed on the VSWR as the main indicator for the quality of the system. First, the transition plus termination was tested separately. The results are shown in Fig. 5-5. Over the range 9.8 - 11.8 KMC the VSWR remains below 1.05. Below 9.8 KMC the VSWR increases slightly to 1.1 and then rises sharply as the cut-off frequency of the guide is approached.

Following this test the entire Faraday rotator was tested. This

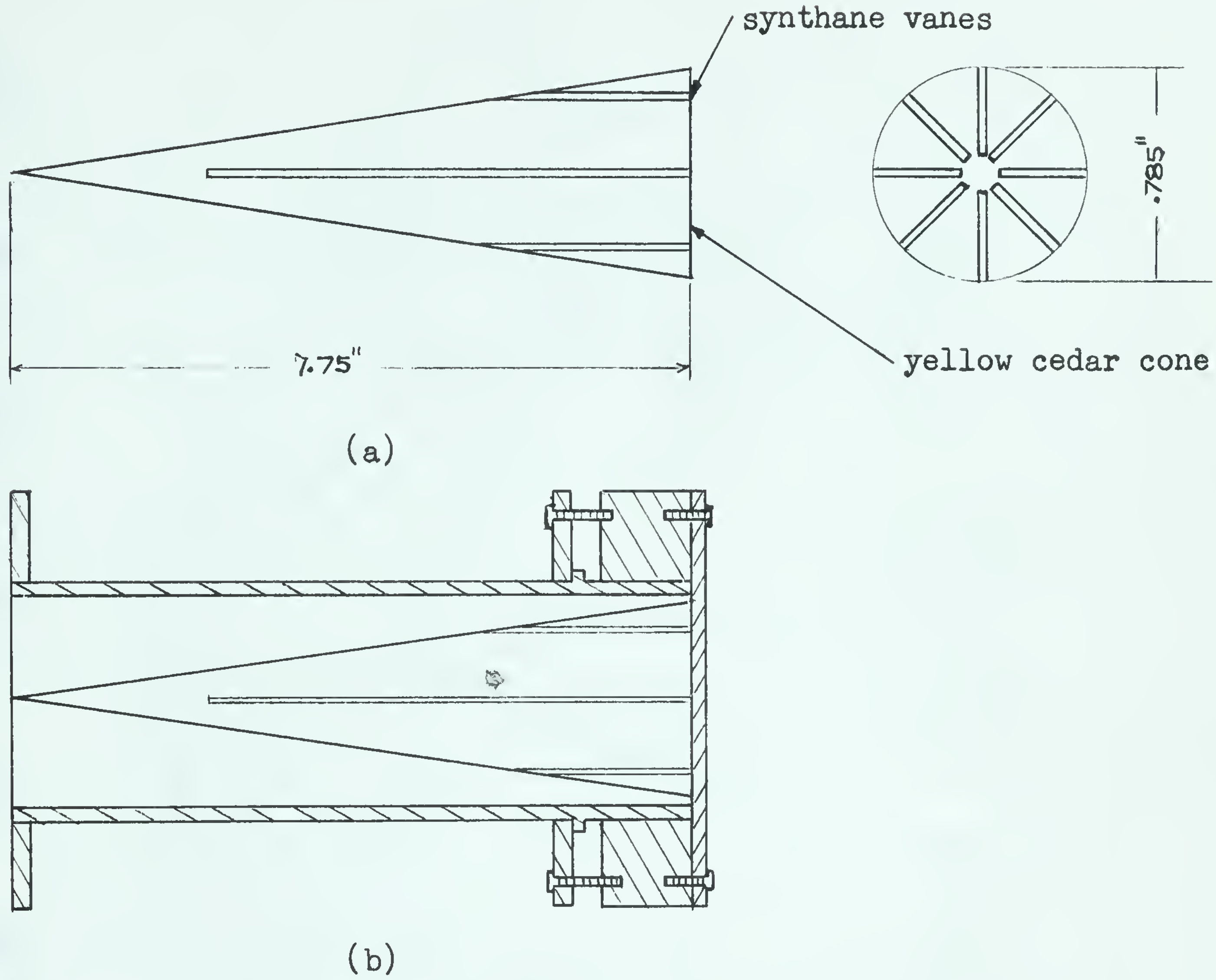

Fig. 5-2 The matched load for the Faraday rotator
(a) the wooden (yellow cedar) cone
(b) the waveguide with cone in place

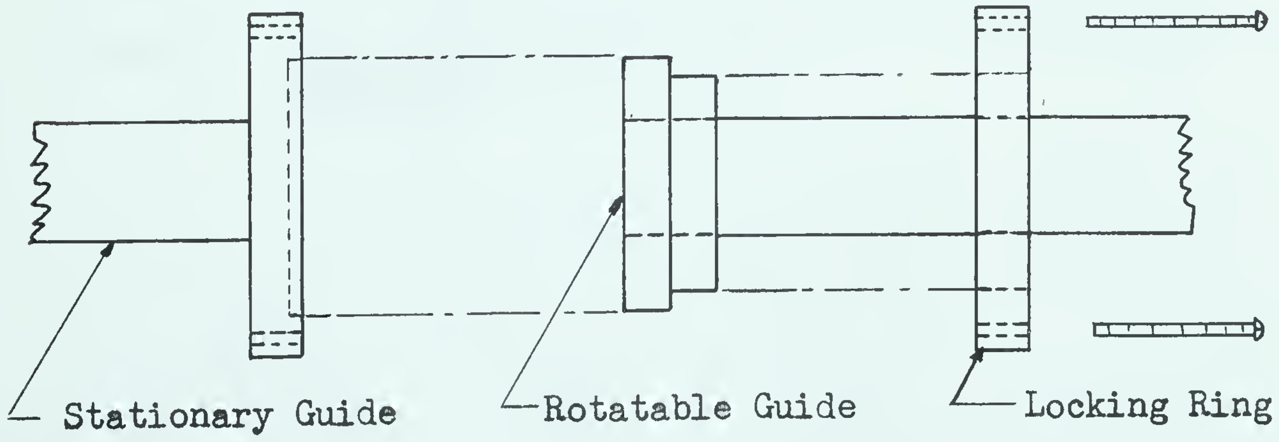

Fig. 5-3. Rotatable Joint

[illegible]

[illegible]

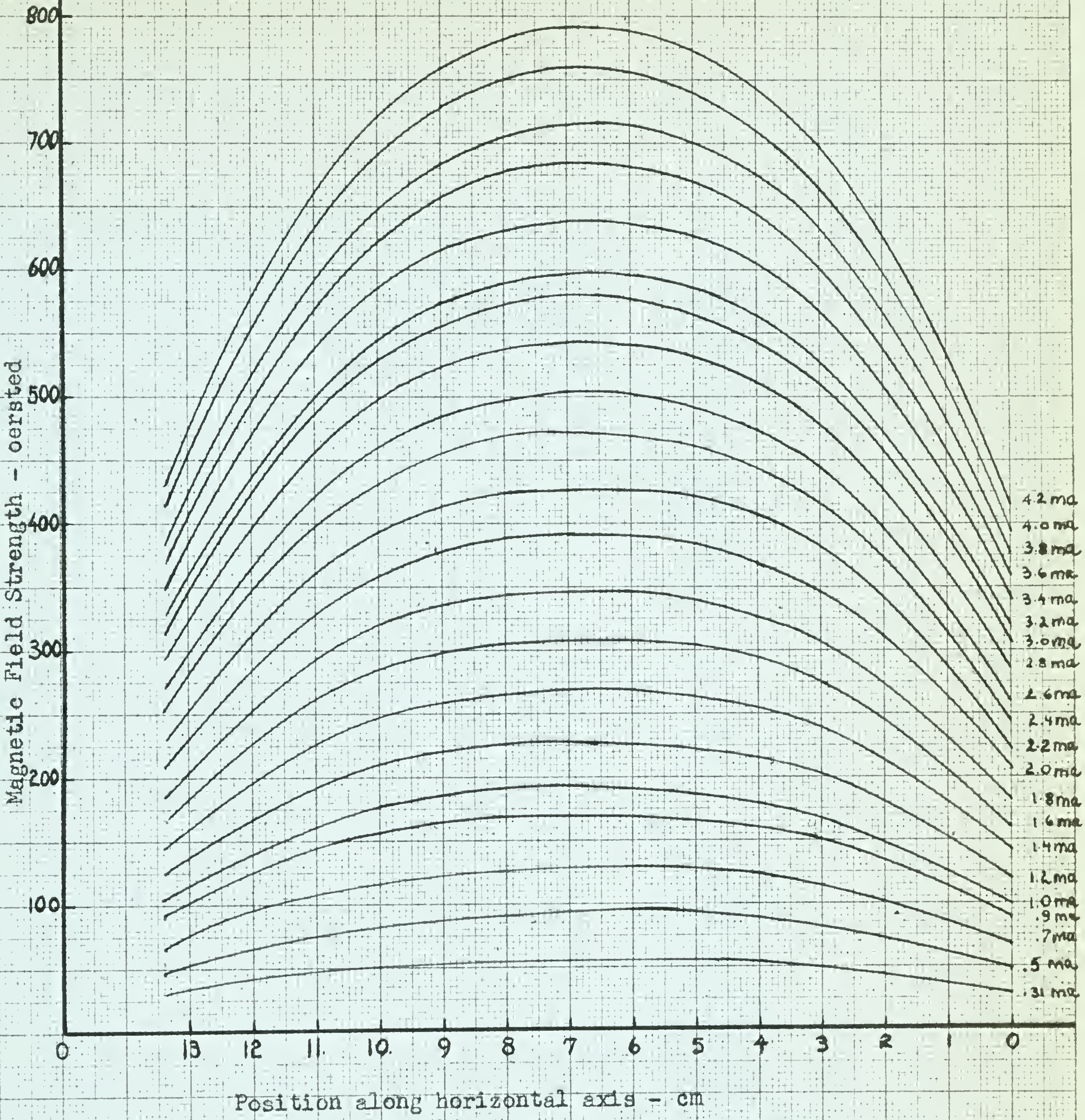

Fig.5-4. Axial distribution of magnetic field strength for the experimental coil # 1.

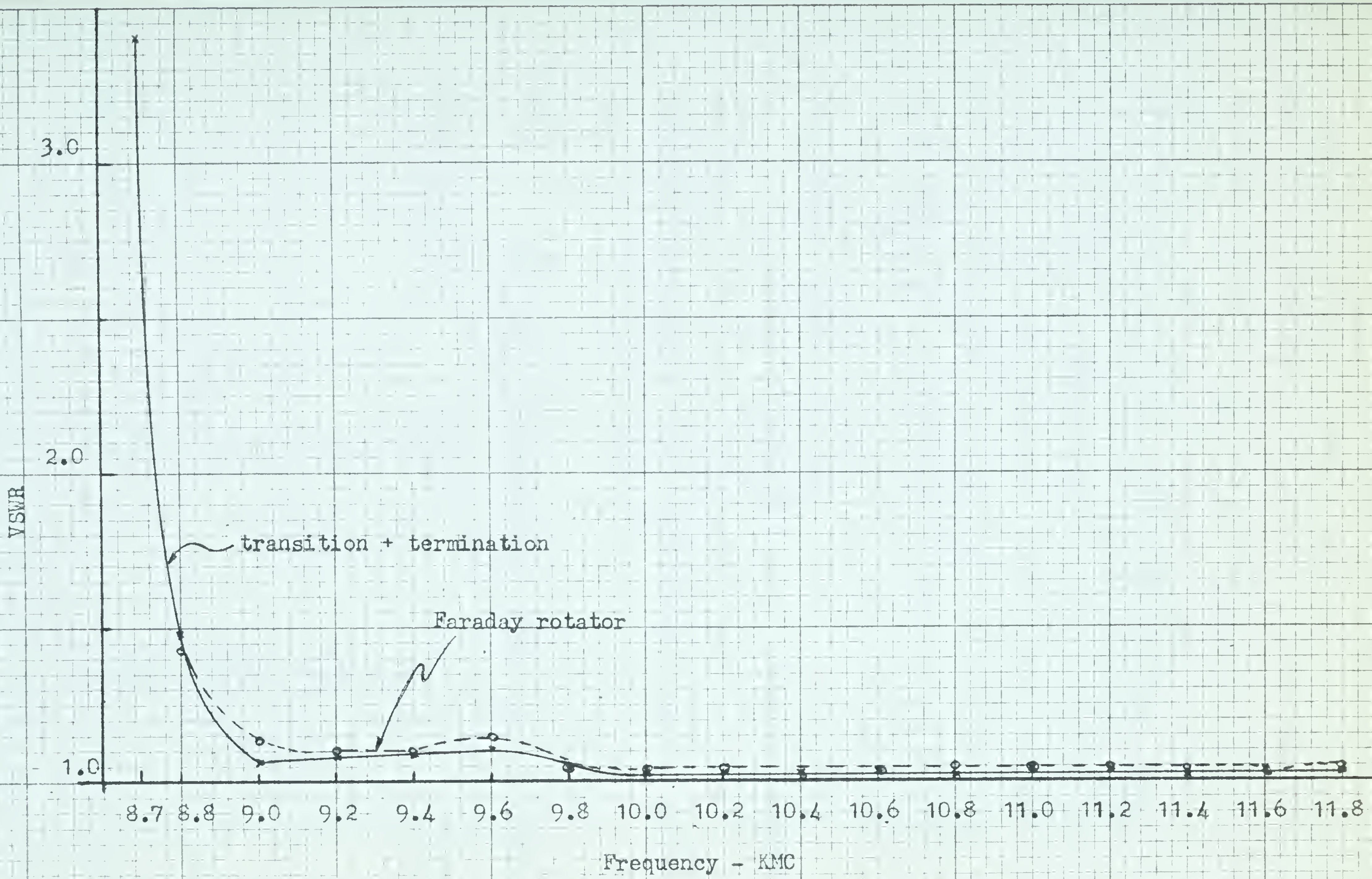

Fig.5-5. VSWR vs.frequency for a) transition + termination, b) Faraday rotator (0mm probe penetration).

time VSWR measurements had to be taken with probe penetration as parameter as it was anticipated that some influence would be exerted on the system by the probe. The results for probe penetrations of 0; 1; 1.5; 2.0; 2.5; 3.0 mm are displayed by Fig. 5-6 and it can be seen that noticeable changes occur only as the probe penetration increases beyond 2.5 mm;even these changes are not very significant. Nevertheless the probe penetration is kept below 2 mm during following tests. Fig.5-5 also shows a comparison of the VSWR of the transition plus termination and that of the Faraday rotator with 0 mm probe penetration. Again the overall VSWR remains below 1.05 for the band 9.8 - 11.8 KMC.

For certain frequencies (9; 10; 11 KMC) and certain probe penetrations (0; 1; 3 mm) the rotatable guide was rotated in 10° steps and the VSWR was recorded to observe the circular property of the system. The results are presented in Table 5-1.

Table 5-1. VSWR measurements for the Faraday rotator at 10° intervals as a function of frequency with probe depth as parameter.

Probe Penetration mm	Frequency KMC	Average VSWR	Maximum Deviation in VSWR
0	9	1.14	.015
	10	1.03	.01
	11	1.04	.015
1	9	1.06	.025
	10	1.04	.015
	11	1.04	.005
3	9	1.23	.15
	10	1.08	.085
	11	1.04	.03

To complete the analysis VSWR measurements were taken with only the termination being rotated. No deviations were noted here .

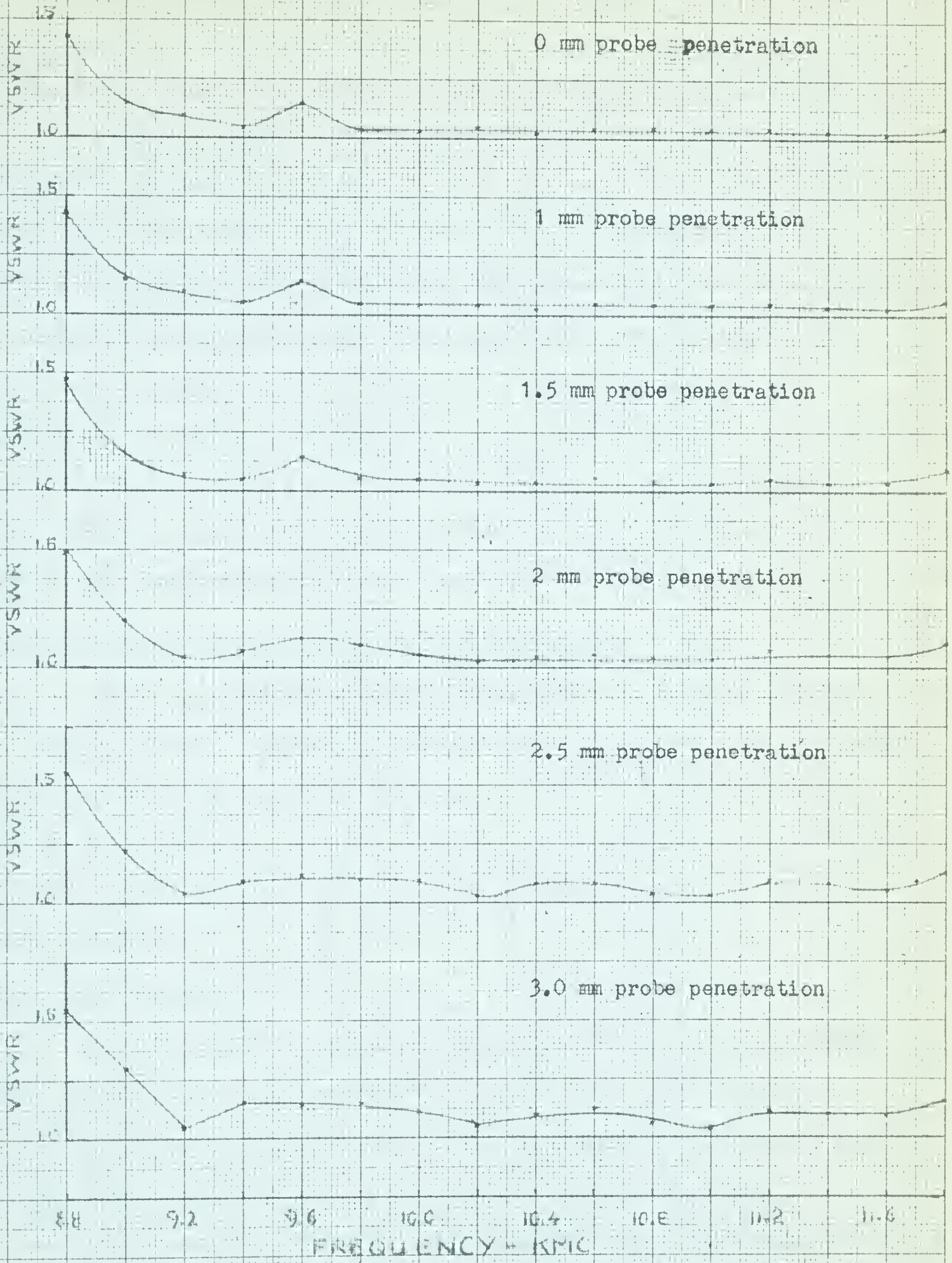

Fig.5-6. VSWR vs. frequency for the Faraday rotator as a function of probe pentration.

5.1.2. Experimental Observations made with the Faraday Rotator.

Faraday rotations as a function of applied dc magnetic field were measured at frequencies of 9; 9.5; 10 KMC. The results are given in Fig.5-7. It should be noted that instead of plotting the curves directly as a function of applied field, they are plotted against coil current as this is the parameter actually measured. The corresponding field strength can be determined from Fig.5-4. It is noted from Fig.5-7 that the rotation increases with increasing frequency in agreement with theory. As the point of saturation is reached the curves level off and the rotation remains almost constant. The curves indicate that reasonable rotations can be obtained for moderate fields (below 100 oe.).

5.2. Experimental Analysis of the A- and B- Sections.

Table 4-3 summarizes design calculations for seven A-sections and four B-sections. The mircrowave performance of these waveguide sections was studied experimentally with the view to select that section giving the best overall performance as the prototype for the modulator. The following describes the test procedures used and the results obtained for the A- and B-sections.

5.2.1. Test Procedures

Only two basic cylindrical brass guide structures with standard X-band guide flanges were manufactured, one for the 2" long B-sections, one for the 4" long A-sections. Complete sets of measurements were obtained for each series starting with the smallest inside guide diameter.

A 5" long magnetizing coil was produced whose inside diameter was large enough to fit over the flanges. The coil consisted of 16,000 turns of #30 wire. Its field distribution along the horizontal axis is given by Fig.5-8.

Each waveguide section was tested for the following four properties:

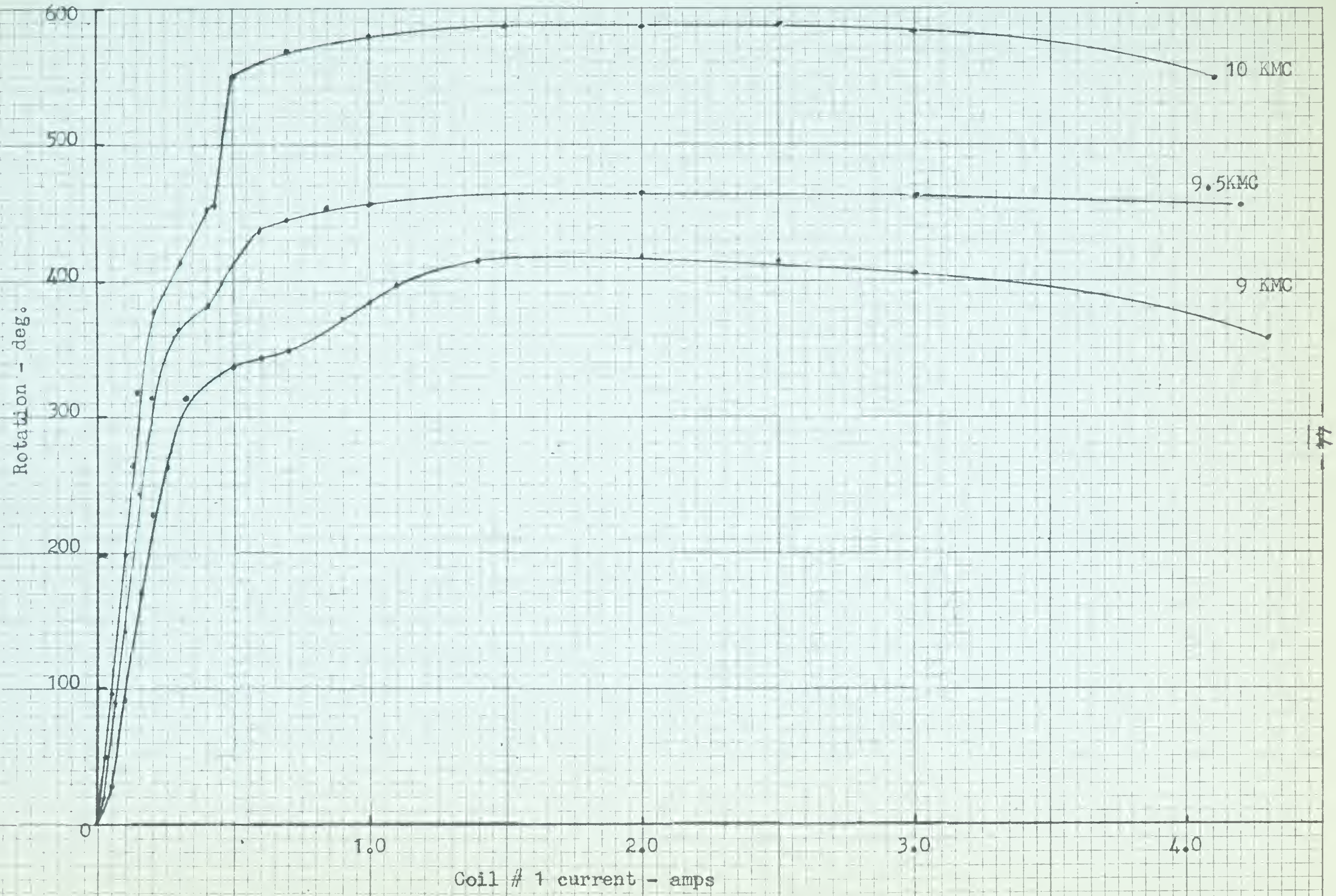

Fig. 5-7. Rotation vs. coil #1 current for a .25" diameter, 2" length, ferrite rod in a .800 in. circular guide.

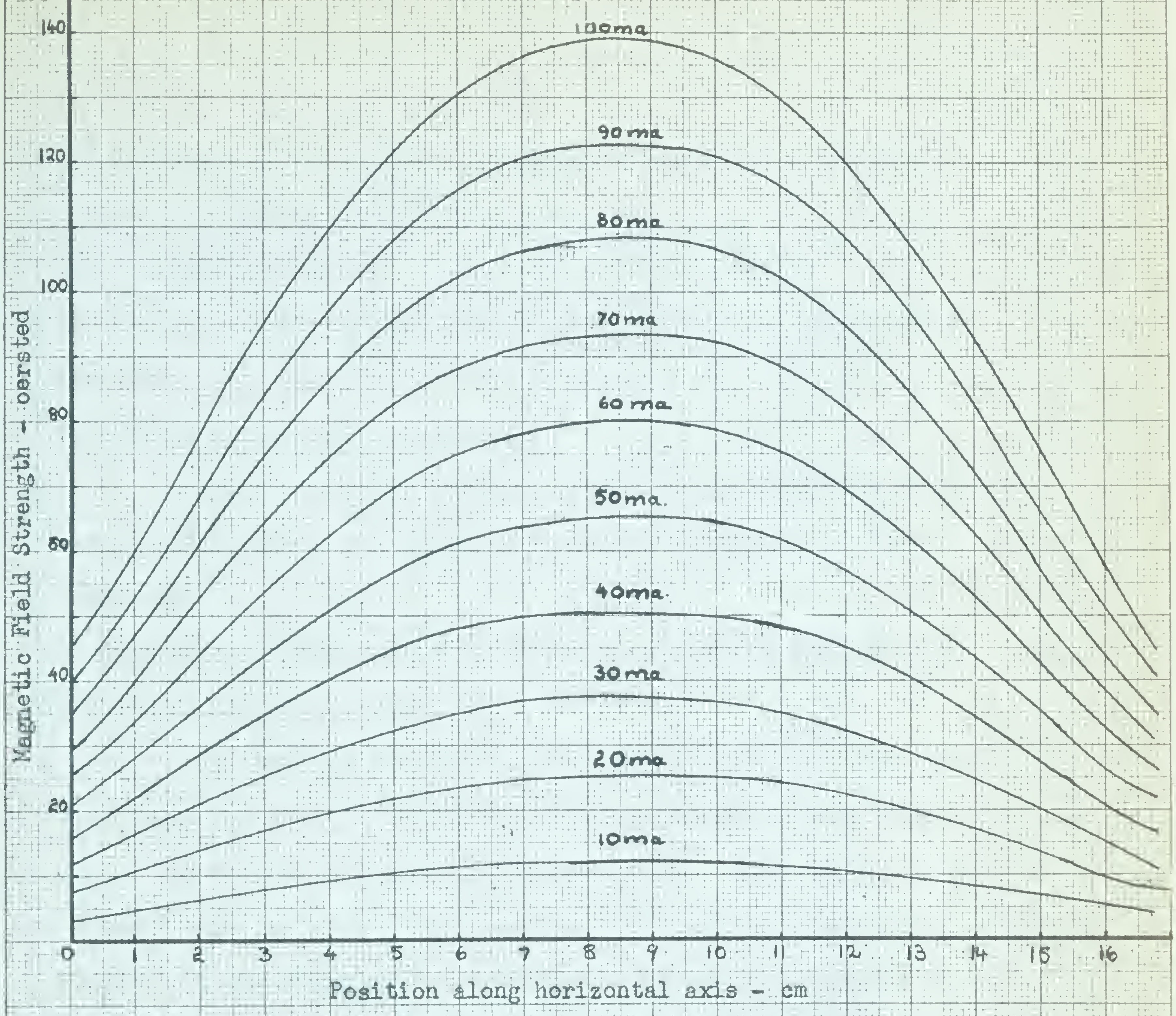

Fig.5-8. Axial distribution of magnetic field strength for the experimental coil # 2.

i) VSWR as a function of frequency,

ii) Variation of transmission of microwave energy as a function of applied dc magnetic field,

iii) Dissipative loss

iv) Maximum attenuation vs. applied dc magnetic field and operating frequency.

i) VSWR as a function of frequency

Standard methods are used to measure the VSWR. The ferrite is demagnetized and the waveguide section is terminated by a standard X-band termination .

ii) Variation of transmission of microwave energy as a function of applied dc magnetic field.

The test set up for measuring this characteristic is shown in Fig. 5-9. The current through the coil is measured as the voltage drop across the precision resistor of 10 ohms ± $\frac{1}{2}$% . This voltage is applied to the X terminal of the X-Y recorder. The output of the crystal detector is fed into the standing wave indicator. The signal appearing at the output of the meter amplifier tube of the hp 415B Standing Wave Indicator is applied to the Y terminal operating in the ac mode. The current through the coil is increased manually and a recording of the transmission characteristics is obtained. Some results are given in Fig.6-12 to 6-15. Assuming square law characteristics for the crystal detector the Y-axis is labelled "relative power output".

iii) Dissipative Loss

The losses due to dissipation only inside the device are determined by the following method (14). The component to be tested is terminated in a movable short. The maximum and minimum VSWR and the locations of their respective voltage minima are determined. It can be shown that

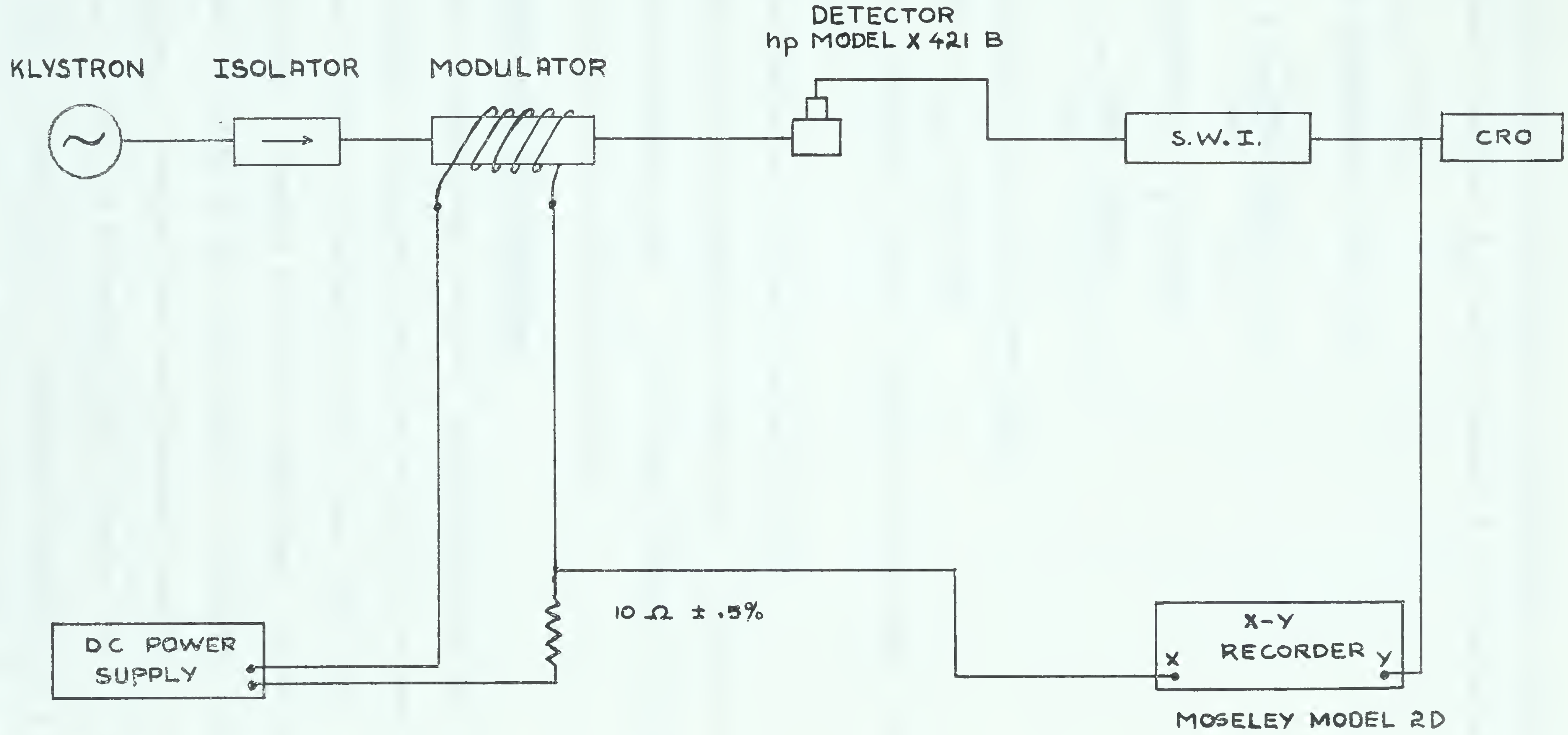

Fig 5-9 Test set up for measuring variations in transmisson of microwave energy as a function of applied dc magnetic field.

only two cases can arise for the location of those minima: either they are at the same place or theyare $\lambda_g/4$ apart, where λ_g is the guide wavelength.

Then $$L_D = 10 \log R$$

where L_D is the dissipative loss in db

$$R = \frac{(r_{max})(r_{min}) - 1}{(r_{max} + 1)(r_{min} + 1)}$$

if the voltage minima are $\lambda_g/4$ apart

and $$R = \frac{r_{max} - r_{min}}{(r_{max} + 1)(r_{min} + 1)}$$

if the voltage minima occur at the same place,

r_{max} = max. VSWR ; r_{min} = min. VSWR

During this test no magnetic field is applied and the sample is in a demagnetized state.

iv) Maximum attenuation vs. applied dc magnetic field.

Attenuation measurements were made using a precision attenuator placed between the modulator and the crystal detector. The method is referred to, at times, as the substitution method.

5.2.2. Test Results for the B-Sections

Table 5-2 summarizes the VSWR measurements for the four B-sections. The VSWR is in general excessively large and only at a few specific frequencies does it take on reasonable values, e.g. less than 3. However, as the guide diameter increases a definite improvement in the VSWR can be noted. To asses the order of this improvement , the VSWR for the individual sections is averaged over the frequency band 8.8 - 11.8 KMC. The averages in the order of increasing guide diameter are 31, 18, 15, 9.6.

In Fig. 5-10 and Fig.5-11 transmission patterns as a function of applied coil current at various frequencies for B-section #4 are shown. These patterns are typical of those for the other B-sections. The initial

Table 5-2. VSWR measurements for the B-sections

f KMC	# 1 VSWR	# 2 VSWR	# 3 VSWR	# 4 VSWR
8.8	70.7	52.4	44.	28.5
9.0	50.	6.	36.	15.7
9.2	54.5	24.5	33.6	12.4
9.4	28.8	24.5	10.1	3.3
9.6	13.6	13.6	5.2	12.6
9.8	54.5	10.8	16.8	2.3
10.0	3.9	22.3	6.8	10.9
10.2	40.6	4.9	10.	2.2
10.4	2.2	21.2	7.8	11.4
10.6	39.5	9.2	14.1	1.3
10.8	11.3	25.2	4.9	11.2
11.0	25.8	13.4	12.8	2.7
11.2	33.7	7.1	1.6	9.8
11.4	3.6	31.8	20.1	10.2
11.6	43.2	5.0	6.1	2.9
11.8	20.6	20.1	11.9	16.8

sharp rise of transmission that can be noted at some frequencies is unexpected and does not fit the derivation of sect.3.2. Further tests revealed that this rise in transmission is also accompanied by a proportional drop in VSWR during the interval up to the first minimum. Fig.5-12 illustrates this behaviour. Since an immediate attenuation is desired as soon as a field is applied, the observed characteristics are not desirable.

Dissipation loss measurements are given in Table 5-3 for B-sections #3 and #4.

Since the VSWR is very high and the transmission characteristics are quite irregular and strongly frequency dependent, the B-sections are excluded from further considerations as a posssible modulator structure.

KEUFFEL & ESSER CO

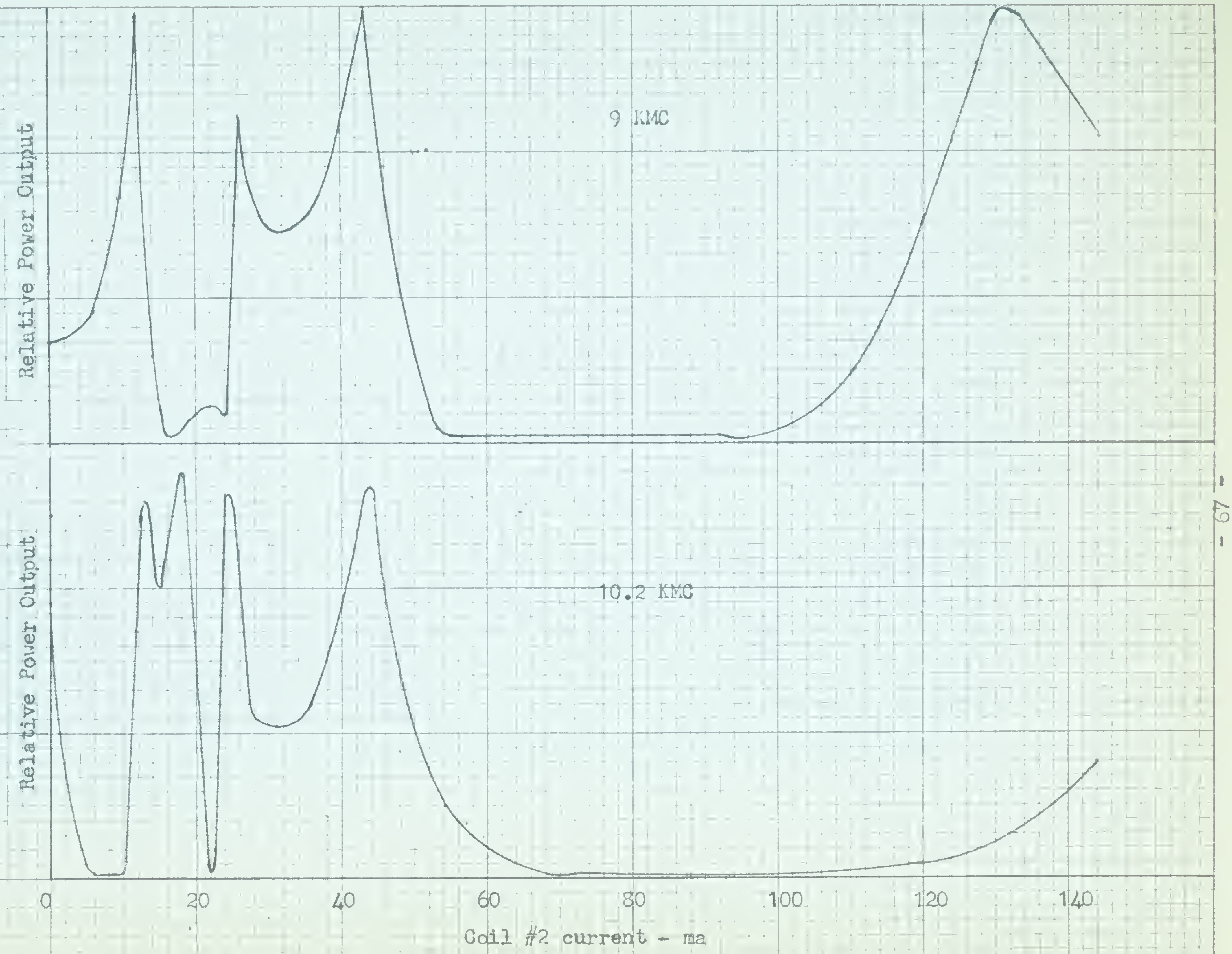

Fig. 5-1 . Transmission characteristics for B-section #4 vs. applied current.

KEUFFEL & ESSER CO.

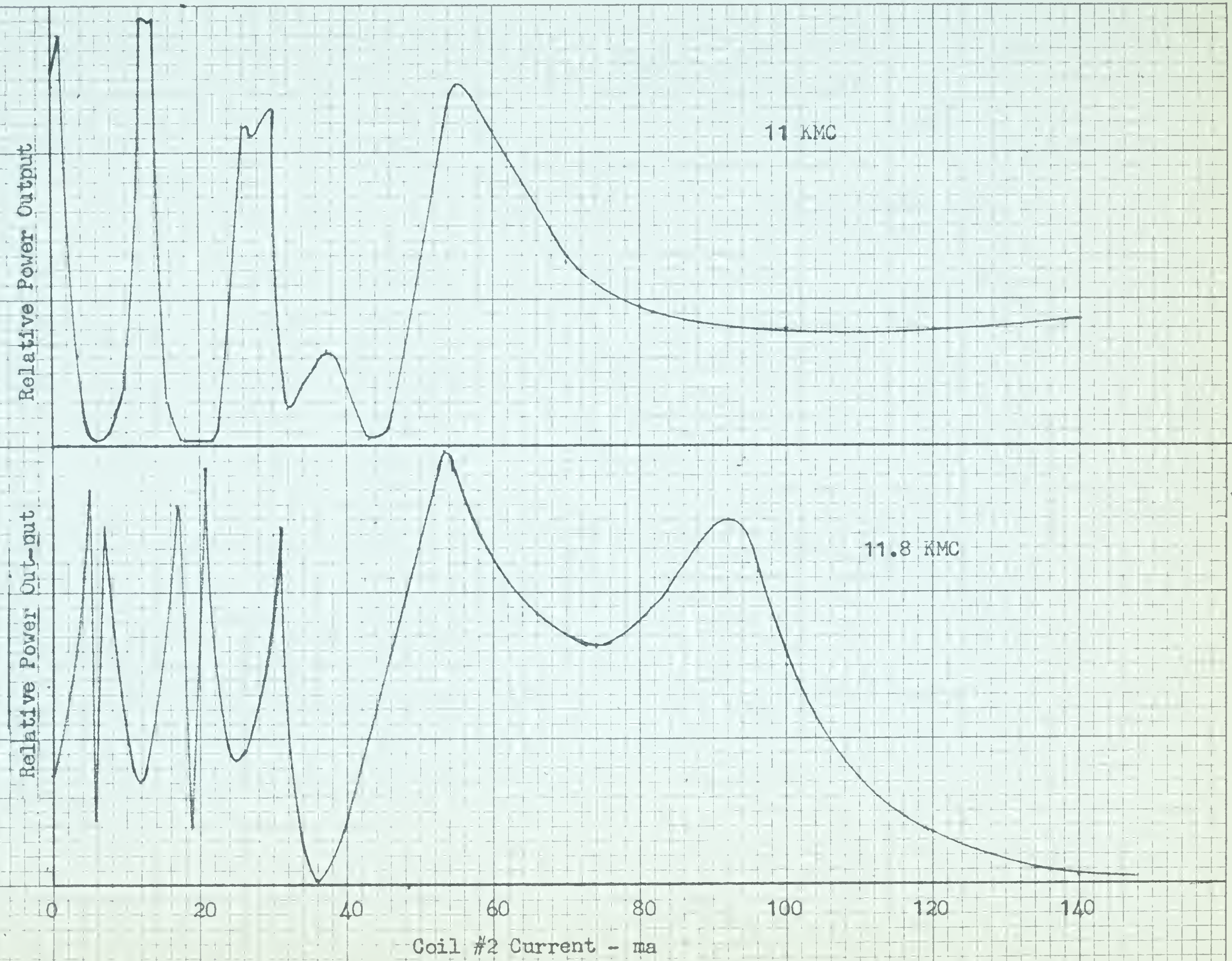

Fig. 5-11. Transmission characteristics of B-section #4 vs. applied current.

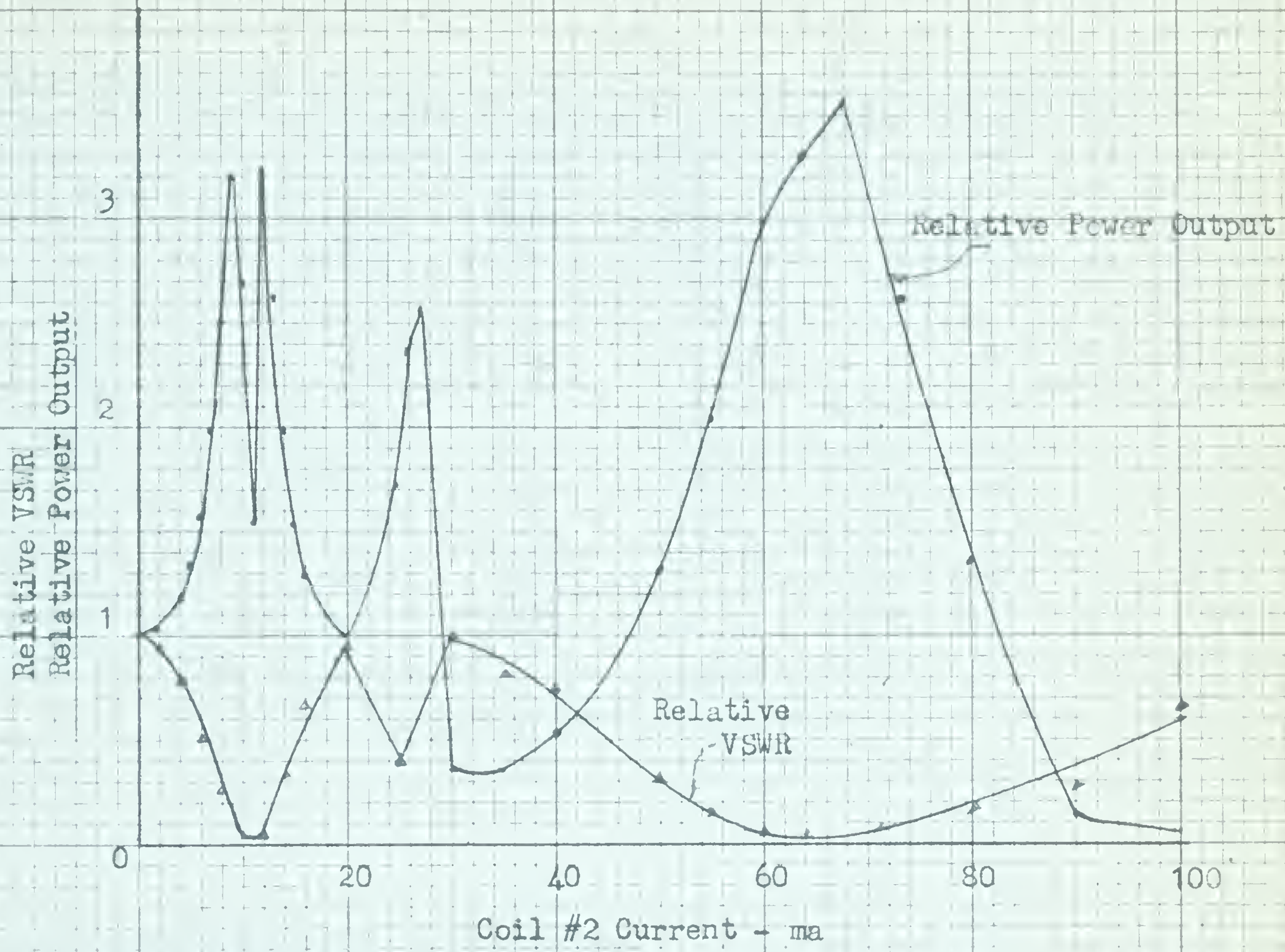

Fig.5-12. Variation of energy transmission and VSWR vs. coil #2 current for B-section #1.

KEUFFEL & ESSER CO.

Table 5-3. Dissipation loss measurements for B-sections #3 and #4

f KMC	#3 Loss db	#4 Loss db
9.4	-	1.42
9.6	2.35	-
9.8	-	3.55
10.2	-	1.57
10.6	-	1.37
10.8	1.35	-
11.2	2.14	-
11.8	-	1.46

5.2.3. Test Results for the A-Sections

The test data for all A-sections are summarized in Table 5-4 to Table 5-7. The recordings of the transmission characteristics are not included for practical reasons. However, their general behaviour can be seen from the curves of the modulator which are included in chapter 6 (Fig.6-12 to Fig.6-15). In evaluating the accumulated data to find the section giving the best overall performance the following method of assigning a figure of merit in the form of a percent value is employed.

From the recordings of the transmission characteristics the upper limit of the operating frequency for each individual section is

Table 5-4. VSWR as a function of frequency (A-sections).

f KMC	# 1 VSWR	# 2 VSWR	# 3 VSWR	# 4 VSWR	# 5 VSWR	# 6 VSWR	# 7 VSWR
8.2				↓ 2.3			↓ 2.1
8.4				1.76		↓ 4.8	2.0
8.6				1.27		1.32	1.1
8.8	58.	11.5	45.3	5.1	10.5	1.13	2.1
9.0	57.3	↓ 2.2	45.7	2.1	↓ 8.56	1.92	2.2
9.2	38.9	3.2	36.8	5.1	1.78	3.75	1.29
9.4	18.1	2.8	32.9	3.0	1.49	1.2	1.62
9.6	7.98	7.0	18.9	1.53	1.43	4.1	2.2
9.8	↓ 2.84	2.8	4.71	1.67	5.40	2.2	↑ 1.55
10.0	1.65	7.0	↓ 1.39	1.04	↑ 1.9	2.0	1.37
10.2	3.11	2.2	4.1	2.0	6.5	2.6	4.1
10.4	2.76	2.6	10.31	↑ 1.48	4.0	1.55	6.5
10.6	4.75	1.7	3.5	3.0	2.1	↑ 1.04	2.8
10.8	3.56	1.9	10.65	4.0	2.3	2.8	9.1
11.0	2.99	↑ 2.5	4.82	1.95	1.34	4.2	2.6
11.2	1.37	4.7	2.2	3.0	1.09	1.26	6.0
11.4	1.32	8.5	2.2	3.9	1.65	5.8	9.5
11.6	1.99	2.4	4.2	2.2	2.3	4.8	6.0
11.8	↑ 4.18	5.6	↑ 3.8	1.36	1.3	1.68	7.3
Avg.VSWR	2.68	3.27	4.82	2.35	3.43	2.3	1.8
% Rating	67.2	55.	37.4	76.6	52.5	78.3	100.

determined. This is done by requiring that the transmission decrease smoothly from its initial values at zero applied field to the first minimum and does not exhibit any kinks, saddles or other irregularities during this interval. The frequency limits thus determined are indicated in the tables by arrow markers to designate the bandwidth in which the particular A-section is considered to operate. An average value of the measurements within the designated bandwidth is next obtained and to that section

Table 5-5. Current requirement for the first transmission minimum (A-sections)

f KMC	# 1 I ma	# 2 I ma	# 3 I ma	# 4 I ma	# 5 I ma	# 6 I ma	# 7 I ma
8.2				↓			↓ 19.
8.4				15.4		↓	17.
8.6						14.8	16.
8.8							
9.0		↓ 11.6		12.5	↓ 11.5	12.2	12.8
9.2							
9.4					10.	10.5	10.9
9.6				10.			
9.8	↓						↑ 9.0
10.0	8.5	9.1	↓ 10.	9.2	↑ 8.3	8.8	8.8
10.2							
10.4			9.5	↑ 7.9			
10.5	8.0	7.9	9.5				
10.6			9.4		8.8	↑ 7.8	6.0
10.8							
11.0	7.6	↑ 7.	10.	8.0	8.2	6.8	5.5
11.2			10.			7.8	
11.4				9.5	8.0		6.0
11.5	7.1		9.9				
11.6							
11.8	↑	8.0	↑ 11.1	7.9	11.5	8.2	3.2
f_o KMC	10.	9.0	10.0	9.0	9.0	9.0	8.54
% $R_a$ting	100.	73.3	85.	68.	73.9	69.6	53.2

giving the best performance for a particular characteristic (e.g. VSWR) the value of 100 % is assigned.

One exception to this method is the current readings for the first transmission minimum. Percentage values are assigned only to the current readings at the first minimum transmission point corresponding to

Table 5-6. Maximum attenuation at the first transmission minimum.
(A-sections)

f KMC	# 1 atten. db	# 2 atten. db	# 3 atten. db	# 4 atten. db	# 5 atten. db	# 6 atten. db	# 7 atten. db
8.2	No			↓			↓ 30.9
8.4	data			35.8		↓	29.3
8.6	were					40.5	
8.8	taken						
9.0	for	↓ 43.5		36.04	↓ 38.5	37.8	30.1
9.2	this						
9.4	section				39.9	48.5	30.2
9.5		34.7					
9.6				33.75			
9.8							↑ 30.7
10.0		34.3	↓ 31.7	31.6	↑ 43.	51.	21.5
10.2							
10.4				↑ 25.			
10.5		42					
10.6			35.5			↑	
10.8							
11.0		↑ 25.6		17.55	35.7	13.8	7.8
11.2			28.				
11.4							
11.5		15.1					
11.6							
11.8			↑ 11.	15.1			
% Rating		81.4	71.2	72.9	91.	100.	67.9

the figures given in Table 4-3. A summary of all % values for each particular section and property is found in Table 5-8. These percentages are added and averaged to indicate the section having the best overall performance. A discussion of these tables will be deferred until chapter 6. Only the observed current requirements to reach the first transmission minimum are

Table 5-7. Dissipative losses (A-sections)

f KMC	# 1 loss db	# 2 loss db	# 3 loss db	# 4 loss db	# 5 loss db	# 6 loss db	# 7 loss db
8.2							3.95
8.4				4.93			
8.6				4.62		2.24	1.18
8.8							
9.0		8.85		4.0	5.27	2.14	1.4
9.2					3.55		
9.4							1.3
9.6				3.54			
9.8							1.32
10.0	7.66		4.57	3.77	2.48	1.68	
10.2		5.45					
10.4							
10.6		4.64	4.81				
10.8							
11.0	7.68			3.77	2.2	2.97	
11.2			3.18				
11.4							
11.6		6.16					
11.8				3.56	2.06		
Avg.loss	7.67	6.31	4.19	4.17	3.87	2.02	1.83
% Rating	23.8	29.	43.7	43.9	47.3	90.6	100.

compared at this point with the previously calculated rotation values at saturation. Applying to the latter calculations the previous percentage rating as well results in the values shown in Table 5-9 which compares the two sets of current values. It is observed that the sequence of increasing current requirements is fairly well followed by the decreasing rotation sequence.

Referring to Table 5-8 A-section #6 shows the highest percent value. Thus this section is chosen as the prototype for the modulator

Table 5-8. Summary of % ratings for the A-sections.

Property	# 1 %	# 2 %	# 3 %	# 4 %	# 5 %	# 6 %	# 7 %
Attenuation	-	81.4	71.2	72.9	91.	100.	67.9
VSWR	67.2	55.	37.4	76.6	52.5	78.3	100.
Current	100.	73.3	85.	68.	73.9	69.6	53.2
Loss	23.8	29.	43.7	43.9	47.3	90.6	100.
Total	191.0	235.7	237.3	261.4	264.7	338.5	321.1
Avg.	63.7	59.	59.3	65.4	66.2	84.6	80.3

Table 5-9. Relative comparison between observed and calculated rotations for the A-sections.

A-section #	% Rating		Order of Sequence	
	calculated	actual	calculated	actual
1	96.	100.	2	1
2	73.2	73.3	4	4
3	100.	85.	1	2
4	66.8	68	6	6
5	88.	73.9	3	3
6	73.	69.	5	5
7	57.	53.2	7	7

whose construction and performance is described in the next chapter.

CHAPTER VI

THE CONSTRUCTION AND PERFORMANCE OF THE FERRITE MICROWAVE AMPLITUDE MODULATOR

6.1 The Construction of the Modulator

At the end of the previous section A-section #6 was chosen as the prototype for the modulator structure. Thus the dielectric supporting material for the ferrite rod is teflon ($\varepsilon = 2.1$) and the 4 in. circular guide has a diameter of .596 in..Fig. 6-1 shows the completed modulator structure.

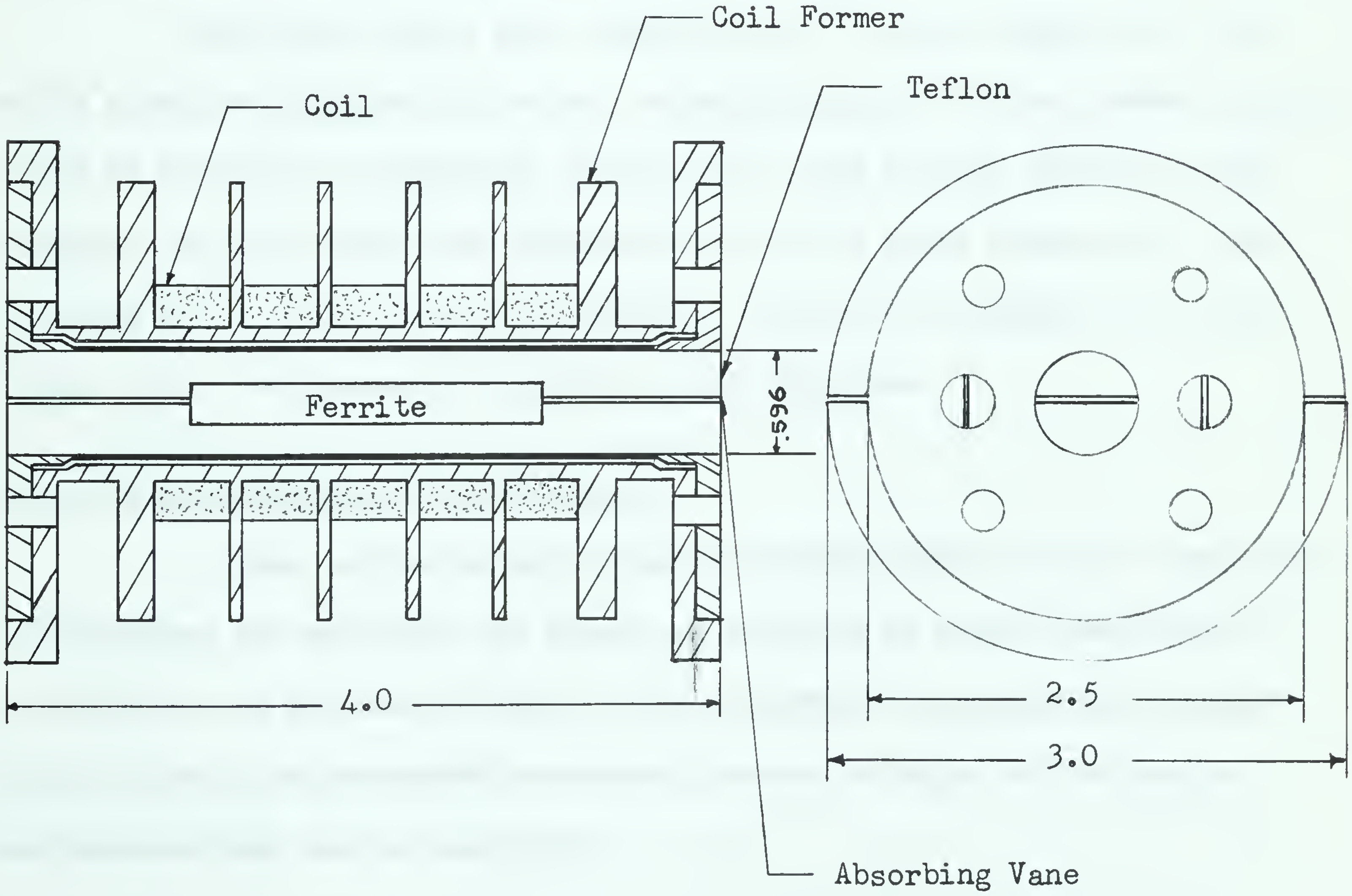

Fig.6-1. The completed ferrite microwave amplitude modulator.

The requirement of a guide wall less than .003" thick necessitated a vastly different construction technique than that which was used for the A-sections as set forth in chapter 5. The very thin film was produced by vacuum depositon of silver followed by electrolytic plating of copper. After some preliminary trials best results were obtained with the following procedure. The teflon rod was sprayed first with a thin coat of liquid acrylic to provide a non-greasy substrate for the vacuum deposition of silver. 4 coats of silver were then vacuum deposited and finally the metal film was built up to about .002"+ with copper in a standard electrolytic bath using copperfluoborate as the electrolyte.

The flanges were designed as shown in Fig.6-1. The collars provide some contact area between the flanges and the teflon rod.

Since the flanges were fitted first, the coil former had to be split along the longitudinal axis. Anticipating that the microwave structure would be sensitive to handling, especially to any torques applied to the flanges, the coil former was designed so that the guide flanges fit into recesses in the ends of the coil former. Bolting the flanges to the coil former lends the necessary rigidity to the structure.

6.2. The Performance of the Modulator

In this section experimentally determined data for the components constituting the modulator are given and compared to either theoretical calculations in the case of the coil or to previous experimental results in the case of the waveguide sections in order to learn to what degree performance data can be predicted.

6.2.1. The Coil Performance

Due to the particular design of the waveguide structure the coil cannot be analysed separately from the guide structure once it is wound on it.

To get around this the coil is wound once with no waveguide structure present. After all measurements are obtained the winding is destroyed. It is assumed that the final coil will be wound in the same manner as the first one and will thus also exhibit the same properties. Table 6-1 compares experimental and calculated values of resistance, inductance, and H_{dc} at the centre of the coil.

Table 6-1. Experimental and calculated data of the modulator coil.

Coil Part	R_{dc} - ohms		L_s - mh		Q	H_{dc} at centre	
	calc.	exp.	calc.	exp.	exp.	calc.	exp.
Sect. #1	10.78	10.5	-	3.78	2.25	18.45	19.6
Sect. #2	10.78	10.6	-	3.85	2.30	18.45	19.8
Sect. #3	10.78	10.6	-	3.84	2.30	18.45	19.3
Sect. #4	10.78	10.6	-	3.76	2.25	18.45	19.9
Sect. #5	10.78	10.6	-	3.84	2.30	18.45	20.0
Entire Coil	53.9	53.4	30.2	30.	3.60	36.6	39.3

R_{dc} = dc resistance
L_s = series equivalent inductance at 1 Kc
Q = quality factor = $\omega L/R$ at 1 Kc
H_{dc} = magnetic field intensity at the centre of the coil or section for a dc current of 100 ma.

The results indicate very good agreement between calculated and experimental values. Fig.6-2 shows the actual field distribution along the axis of the coil for a current of 100 ma. Over the region of the ferrite the curve can be approximated closely by two parabolas. The one to the left of the centre line is given by $H = 39.5 - 1.125\,x^2$, the one to the right by $H = 39.5 - 1.86\,x^2$, where x is measured from the centre line. The average distribution given by $\frac{\int_{-L/2}^{+L/2} H(x)\,dx}{L} = 36.3$ oe.

After removing the coil windings and assembling the coil

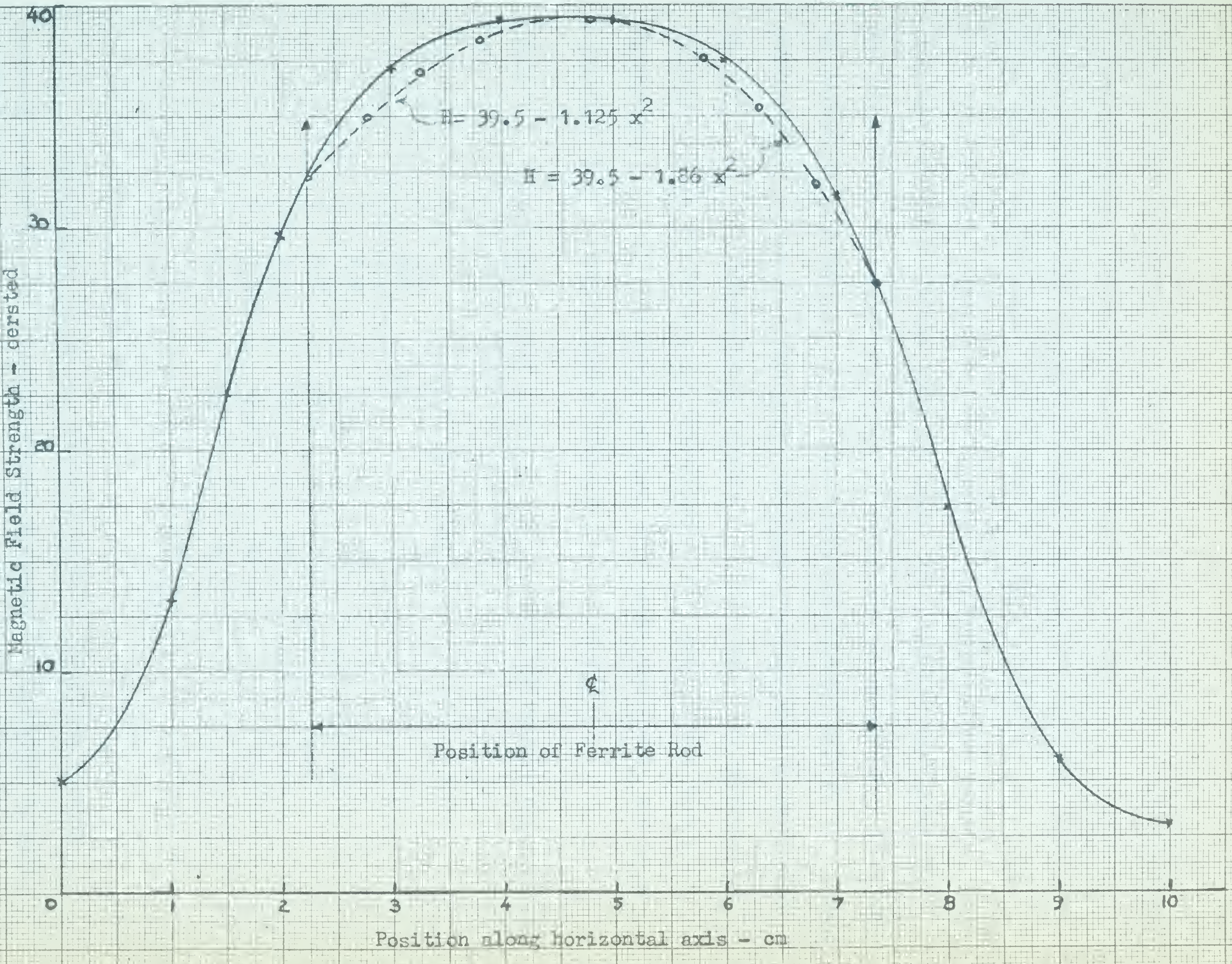

Fig.6-2. Axial distribution of magnetic field strength for the modulator coil

former around the waveguide structure, the coil is re-wound to complete the actual modulator. The current values required to reach the first transmission minimum for the finished modulator are then obtained and compared to those for the experimental A-section #6, in order to learn how closely the same results can be reproduced. To do this a correction factor must be applied since two different coils are used. The modulator coil gives 36.3 oe. for 100 ma, the experimental coil #2 gives 138 oe. for 100 ma. Therefore, to convert current readings taken while using experimental coil #2 to readings corresponding to the modulator coil, the former readings must be multiplied by 138/36.3 . The comparison is tabulated in Table 6-2. The agreement is relatively good considering all the variables that would affect such a comparison (e.g. the many meter readings, Hall probe positions), and it is concluded that reasonable reproducibility can be achieved.

Table 6-2. Comparison between modulator and A-section #6 current requirements for the first transmission minimum.

f KMC	A-sect. #6 I ma	Modulator I ma
8.6	56.2	50.
9.0	46.4	42.
9.4	40.	35
10.0	34.4	30
10.6	29.6	28
11.0	25.8	24

6.2.2. The Modulator Performance

Before considering the modulator alone a comparison between respective data for the A-section #6 and those for the modulator is made, and where appropriate, comparisons are made with the results for the other A-sections.

i) Maximum Attenuation

Table 6-3. Maximum attenuation obtainable with the modulator and A-section #6.

f KMC	A-sect. #6 atten. db	Modulator atten. db
8.6	40.5	30.5
9.0	37.8	30.5
9.4	48.5	35.3
10.0	51.	31.6

Table 6-3 shows a comparison between maximum attenuation values obtained with the modulator and A-section #6. It is stated (ref.4, p.557) that the maximum attenuation possible is a function of the eccentricity of the microwave field inside the guide. Since the A-sections are geometrically more rigid than the modulator, the difference in attenuation is attributed mainly to the physical differences in the two structures. Such differences are possible wall porosity in the thin modulator guide wall, eccentricity of the ferrite rod.

ii) Dissipative Losses

Table 6-4. Dissipative losses in the modulator and A-section #6.

f KMC	A-sect. #6 loss db	Modulator loss db	2nd Sect.#6 loss db
8.6	2.24	2.6	2.29
9.0	2.14	2.85	2.19
10.0	1.68	2.96	1.88
11.0	2.97	4.19	3.66

These losses are high. Since they are higher for the modulator than for A-section #6 another similar section was machined and tested for losses to see whether loss figures are reproduced if the same construction techniques are used. The results indicate that reproducibility is good

(see Table 6-4 column headed 2nd Sect.#6) and therefore the additional losses in the modulator are attributed to the plated waveguide surface and possible radiation losses due to surface porosity.

To account for the absolute magnitude of the losses Table 5-7 is reconsidered. In the order of increasing diameter, the average losses for the A-sections are 7.67 db, 6.31db, 4.19 db, 4.17 db, 3.87 db, 2.02 db, 1.83 db. Clearly the losses decrease as the waveguide diameter to ferrite rod diameter ratio increases. This behaviour is consistent with theory and it appears that even with a ferrite rod to waveguide diameter ratio of .4 attenuation is high.

iii) VSWR measurements are compared using Fig.6-3 which is self-explanatory. It is interesting to note that the general behaviour of the curves is the same except for an apparent shift in frequency..

The modulator overall microwave performance can be seen best by referring to Fig.6-4 and Fig.6-5. From these curves it is contended that except for the rather high VSWR's at 9.1; 9.5; 9.6 KMC the modulator can be used from 8.4 - 10.6 KMC. Over most of this range the maximum attenuation possible at cut--off is better than 30 db . Fig. 6-6 is included to show that for low VSWR the variation in VSWR with applied field does not change greatly. For large VSWR there is an appreciable drop in VSWR as the applied field is increased.

The modulating performance of the modulator is studied by applying a 1 Kc pulse signal to the grid of the 807 vacuum tube as shown in Fig.4-8. The waveforms of the coil current and the corresponding microwave response are shown in Fig.6-7 to Fig.6-11 for several microwave frequencies. It is observed that the character of the current as well as the response waveforms does not change as the microwave frequency is increased. To study the respective rise and fall times the corresponding waveforms at a frequency of

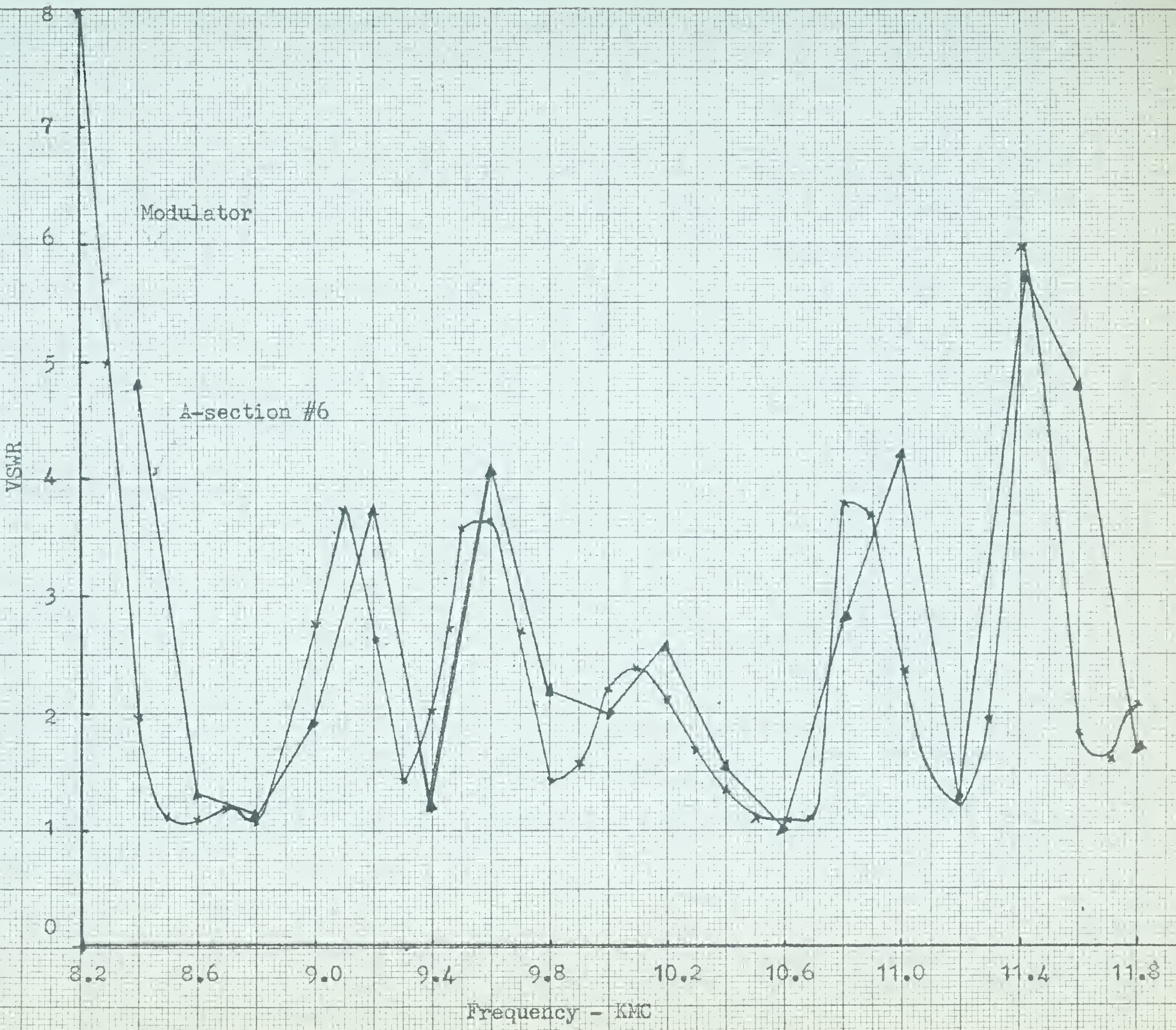

Fig.6-3. VSWR of modulator and A-section #6 as a function of frequency.

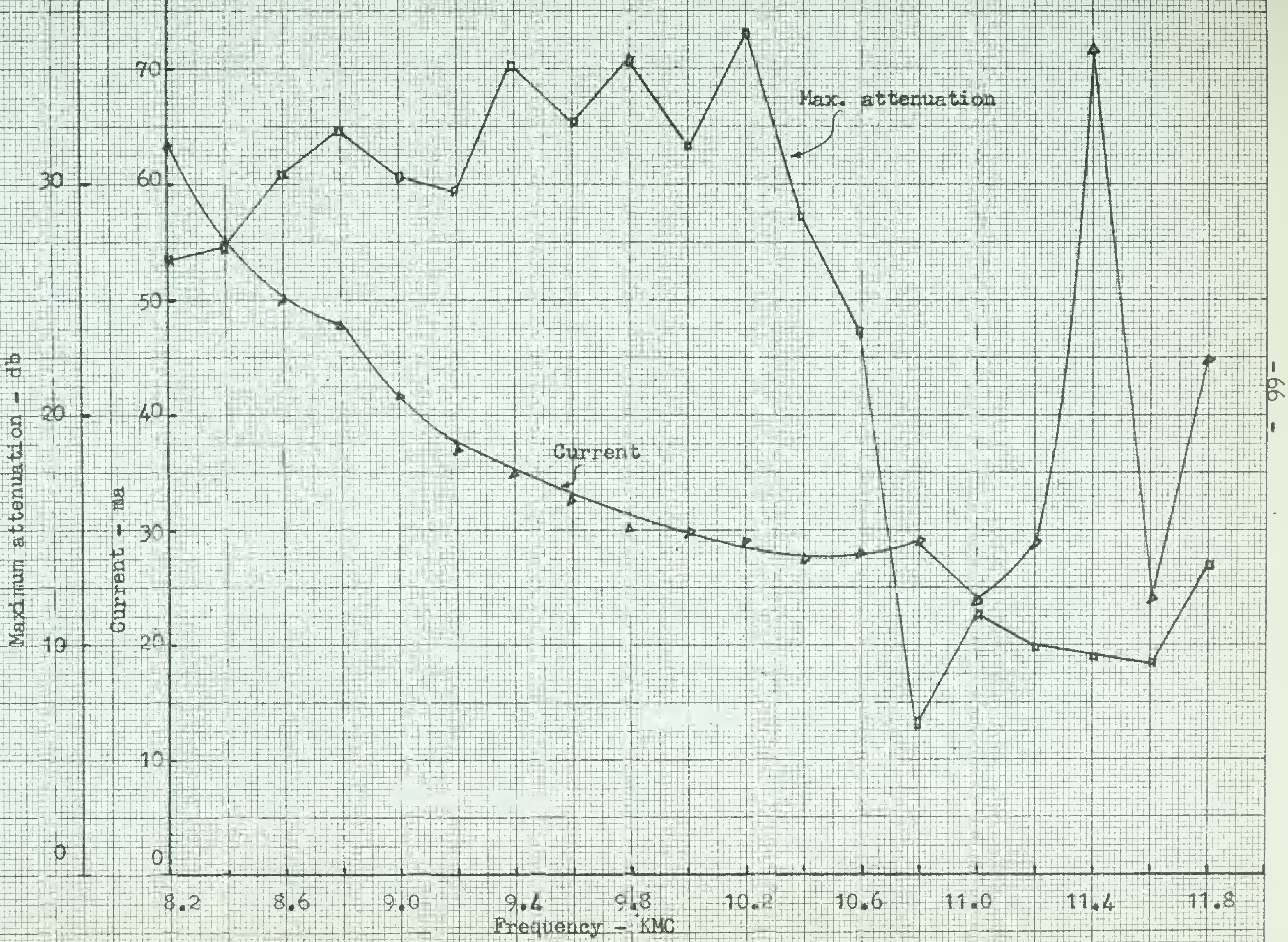

Fig. 6-4. Current requirement for the first transmission minimum and maximum attenuation vs. frequency.

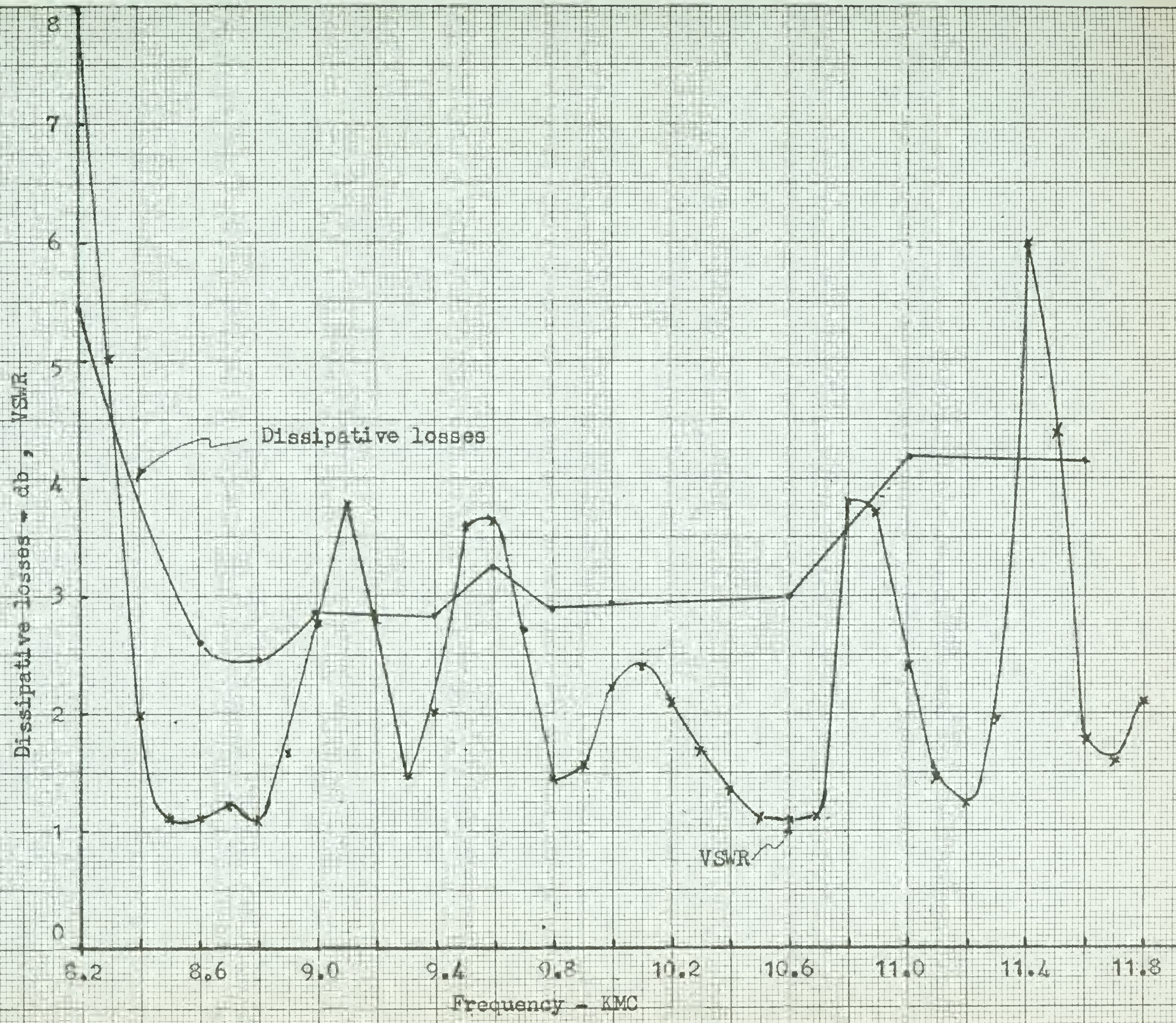

Fig.6-5. VSWR and dissipative losses in the modulator as a function of frequency.

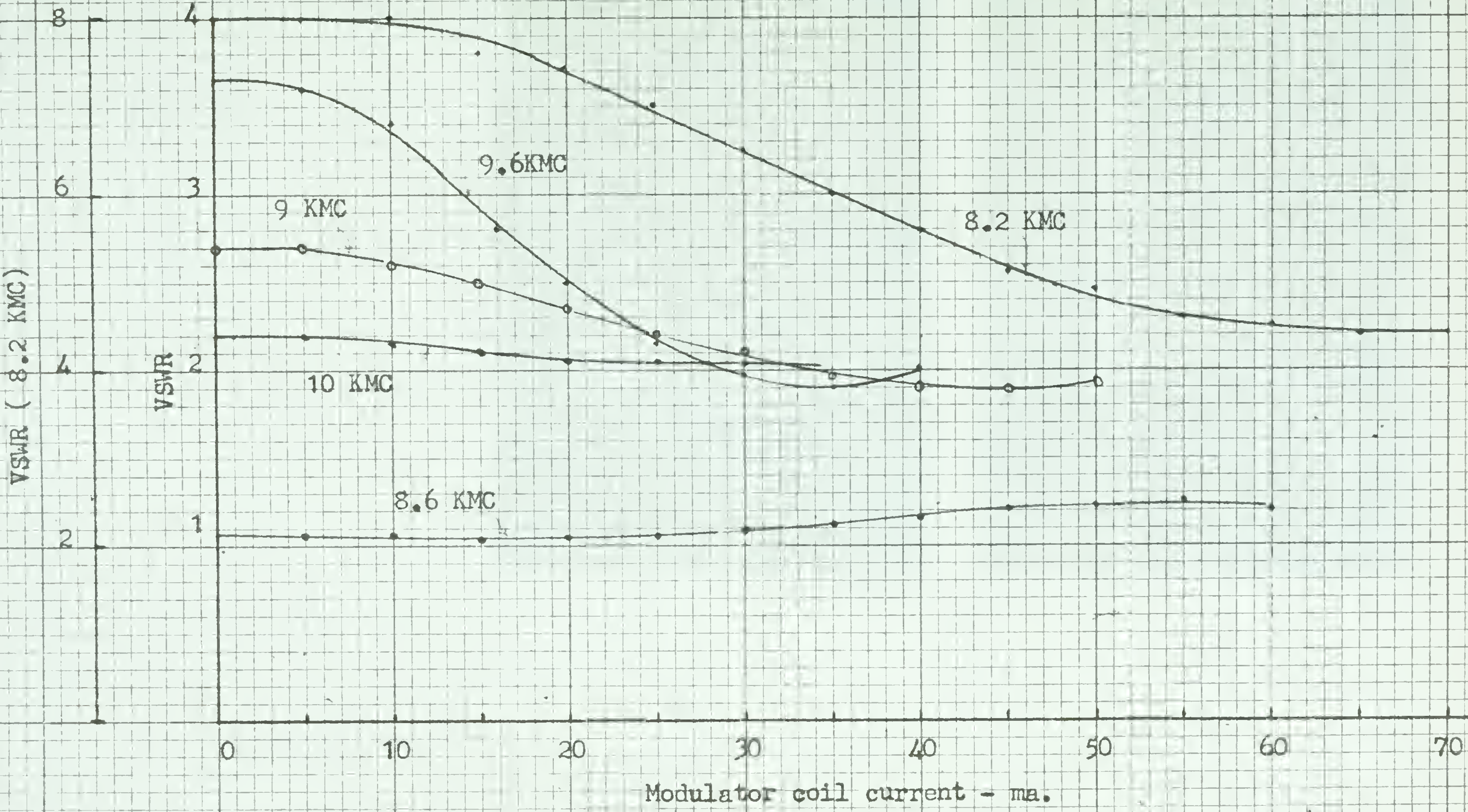

Fig.6-6. VSWR of the modulator as a function of coil current.

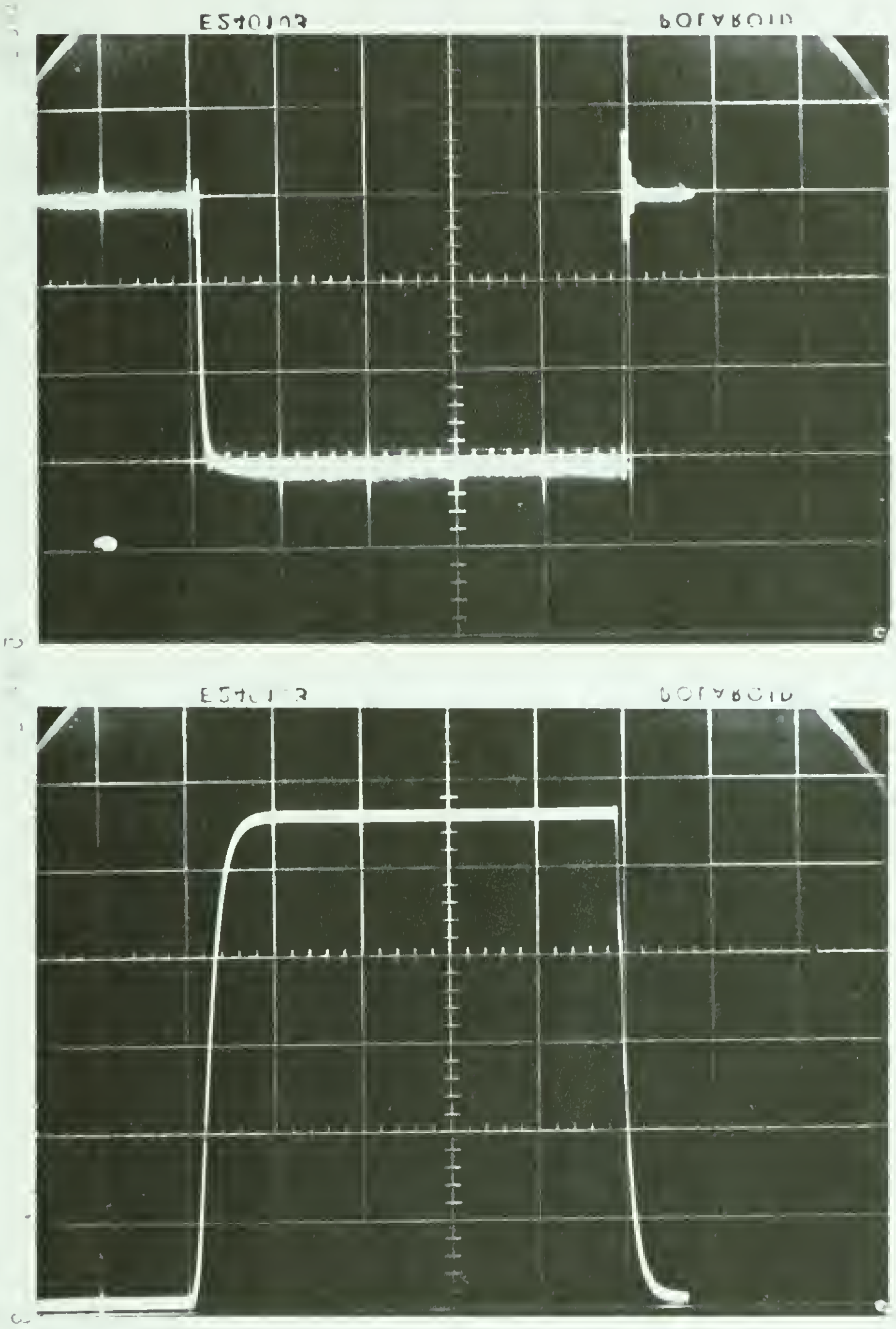

(a) Coil current response ([illegible] ma/cm)

(b) Microwave response

Time scale: .1 msec/cm

Fig. 6-7. Pulse modulation of the modulator at [illegible] KMC

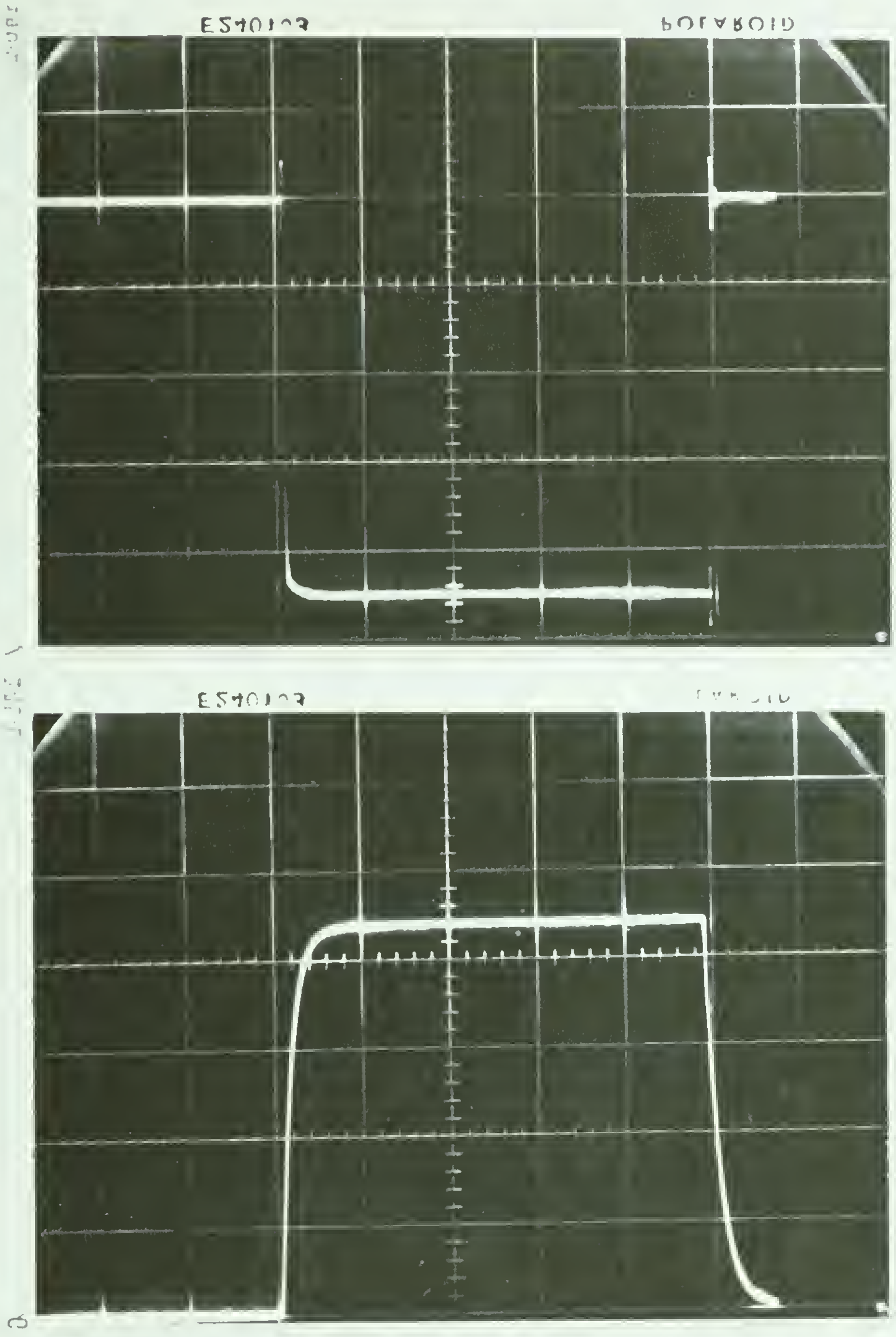

(a) Coil current response (10ma/cm)
(b) Microwave response (5mv/cm)
Time scale: .1msec/cm

Fig.6-[illegible]. Pulse modulation of the modulator at [illegible] KHz.

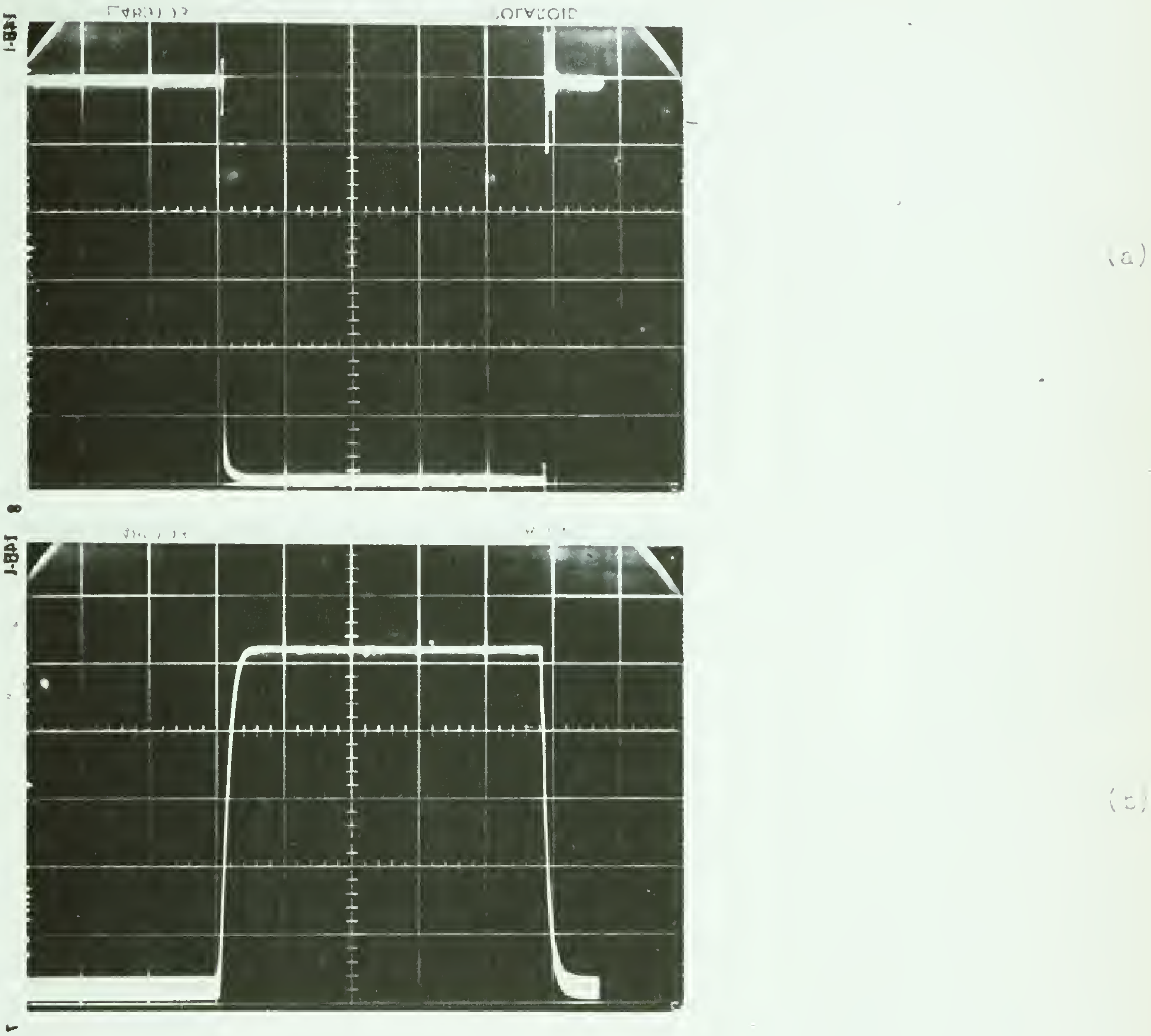

(a) Cell current response (5ma/cm)
(b) Microwave response (2mv/cm)
Time scale: .1msec/cm

Fig.[illegible]-9. Pulse modulation of the modulator at [illegible]

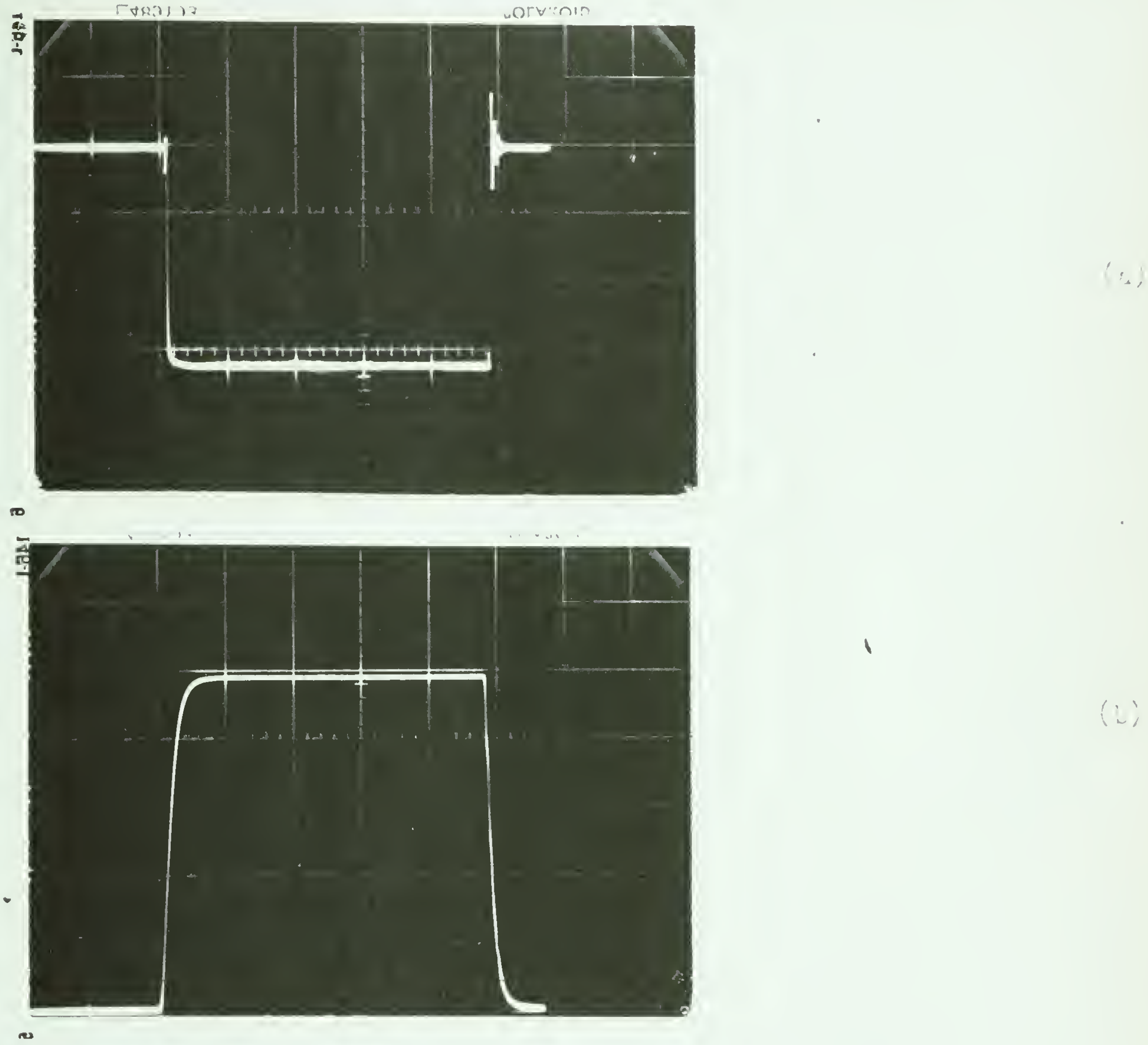

(a) Coil current response

(b) Microwave response

Time scale: .1msec/cm

Fig.6-17. Pulse modulation of the modulator at 11 kMC.

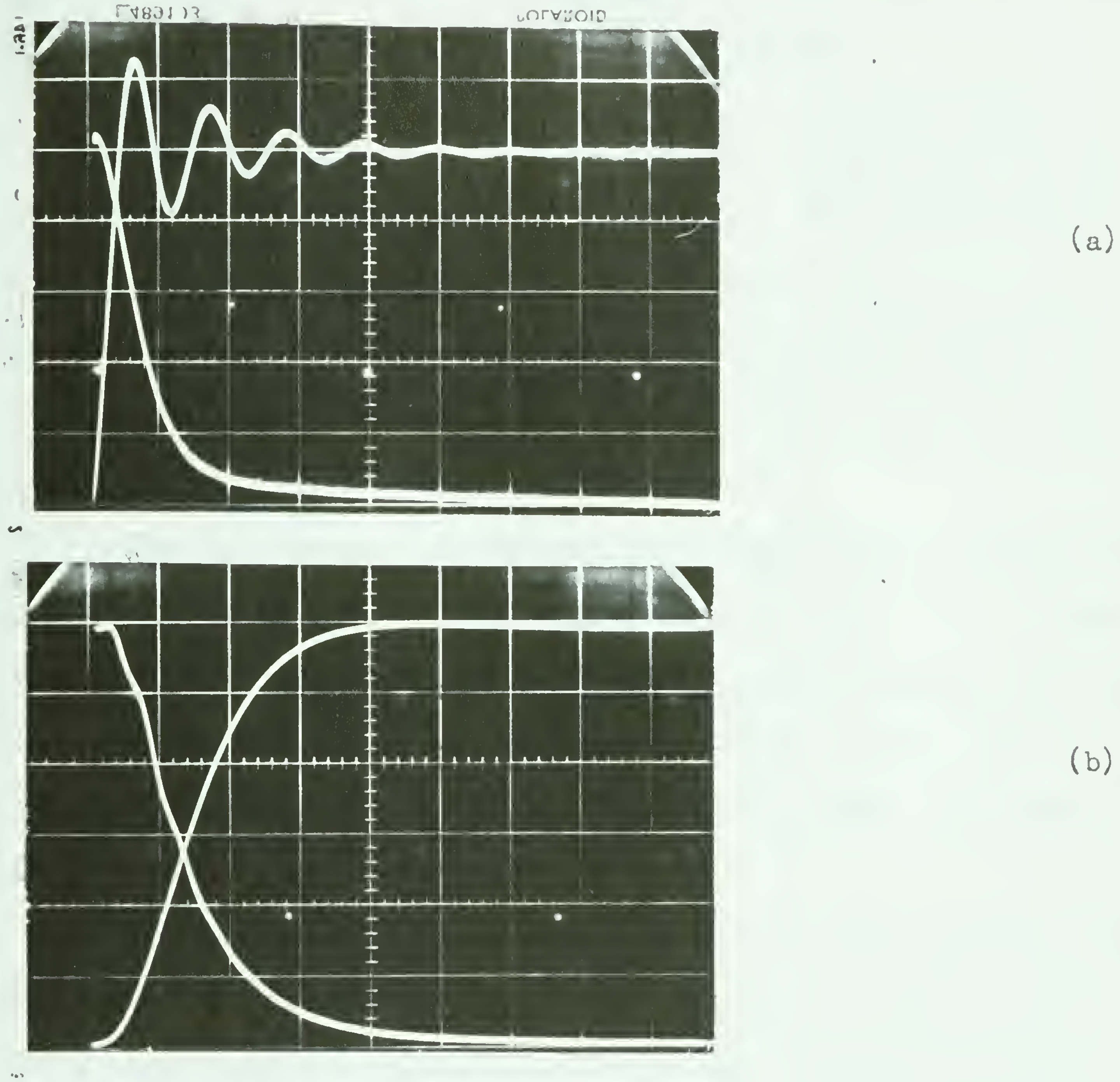

(a) Coil current response

current scale: 10 ma/cm
time scale : 5 usec/cm

(b) Microwave response

response scale : 10 mv/cm
time scale : 10 usec/cm

Fig.6-11. Pulse modulation of the modulator at 9 KMC. (expanded time scale)

9 KMC are presented in Fig.6-11 with anexpanded time scale. From these curves the following rise and fall times are obtained

Current Waveform	Microwave Response
fall time = 6 μsec.	rise time = 21 μsec.
rise time = 2 μsec.	fall time = 20 μsec.

The self-resonance frequency of the coil circuit is found to be 200 Kc. Calculating from this value the capacitance of the driver plate circuit using the measured inductance value of 58 mh for the coil plus ferrite yields a value of C= 10.9 μμf.

The difference in the fall and rise times for the current waveforms is probably due to the fact that during the fall interval the current drops from a region of relatively low plate resistance and therefore relatively long time constant toward cut-off, whereas during the rise period the current increases from a region of relatively high plate resistance and therefore short time constant.

The corresponding much longer rise and fall times of the microwave response are explained as follows (8). The rise and fall times are a function of the high frequency components of the pulse. Considering the coil to be driven by each of the fixed frequencies making up the pulse signal, electromagnetic waves can be imagined to travel from the inside surface of the coil toward the ferrite. As these waves hit the wave guide wall, currents are set up whose values decrease exponentially. Since the skin depth decreases with increasing frequency the higher frequency components are more highly attenuated than the low ones. Therefore, the guide surface acts as a low pass filter and correspondingly the rise time of the microwave response increases. The same mechanism accounts for the fact that the rise and fall times for the microwave response are nearly equal whereas the current rise time is three times shorter than the fall time.

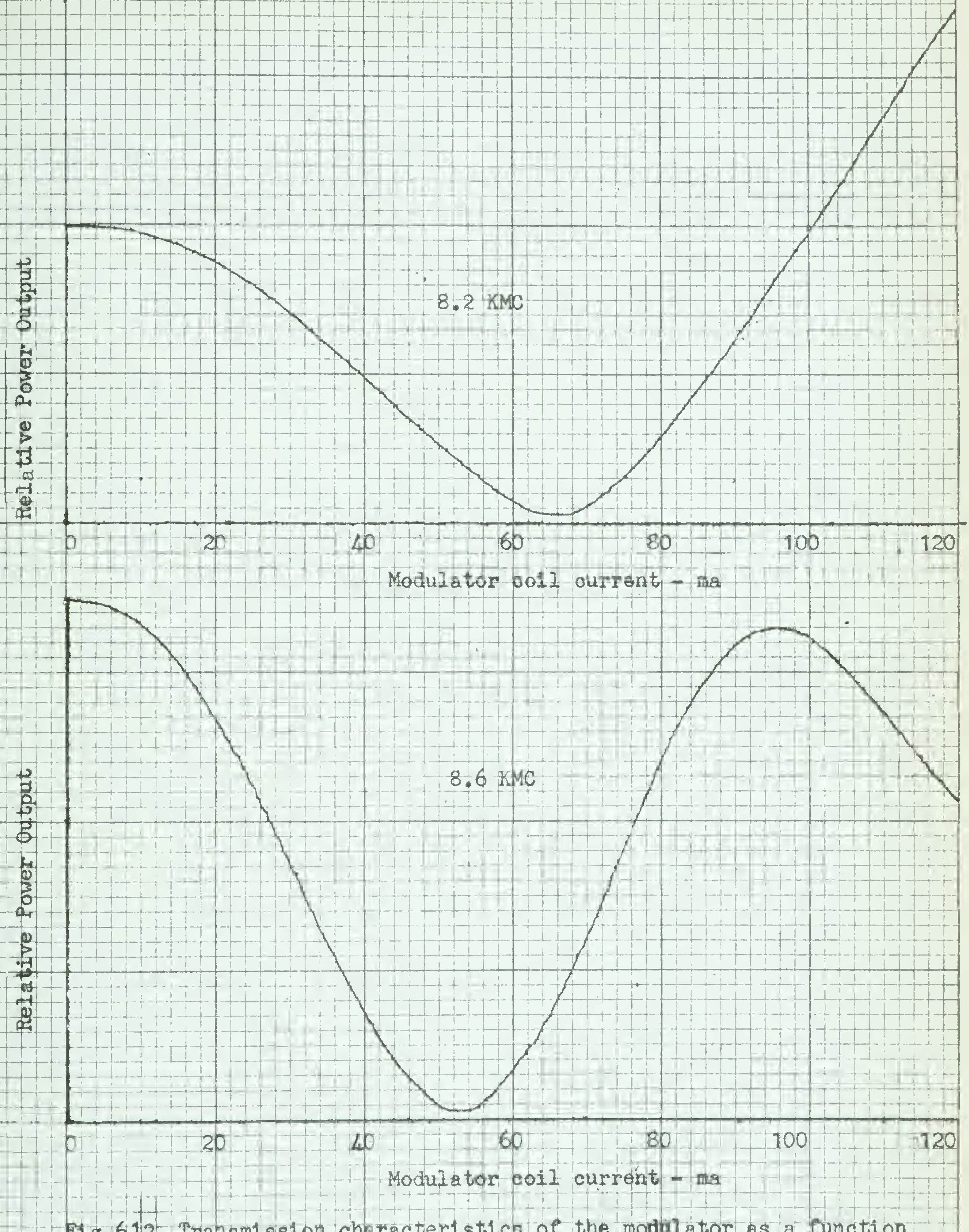

Fig.6-12. Transmission characteristics of the modulator as a function of applied current

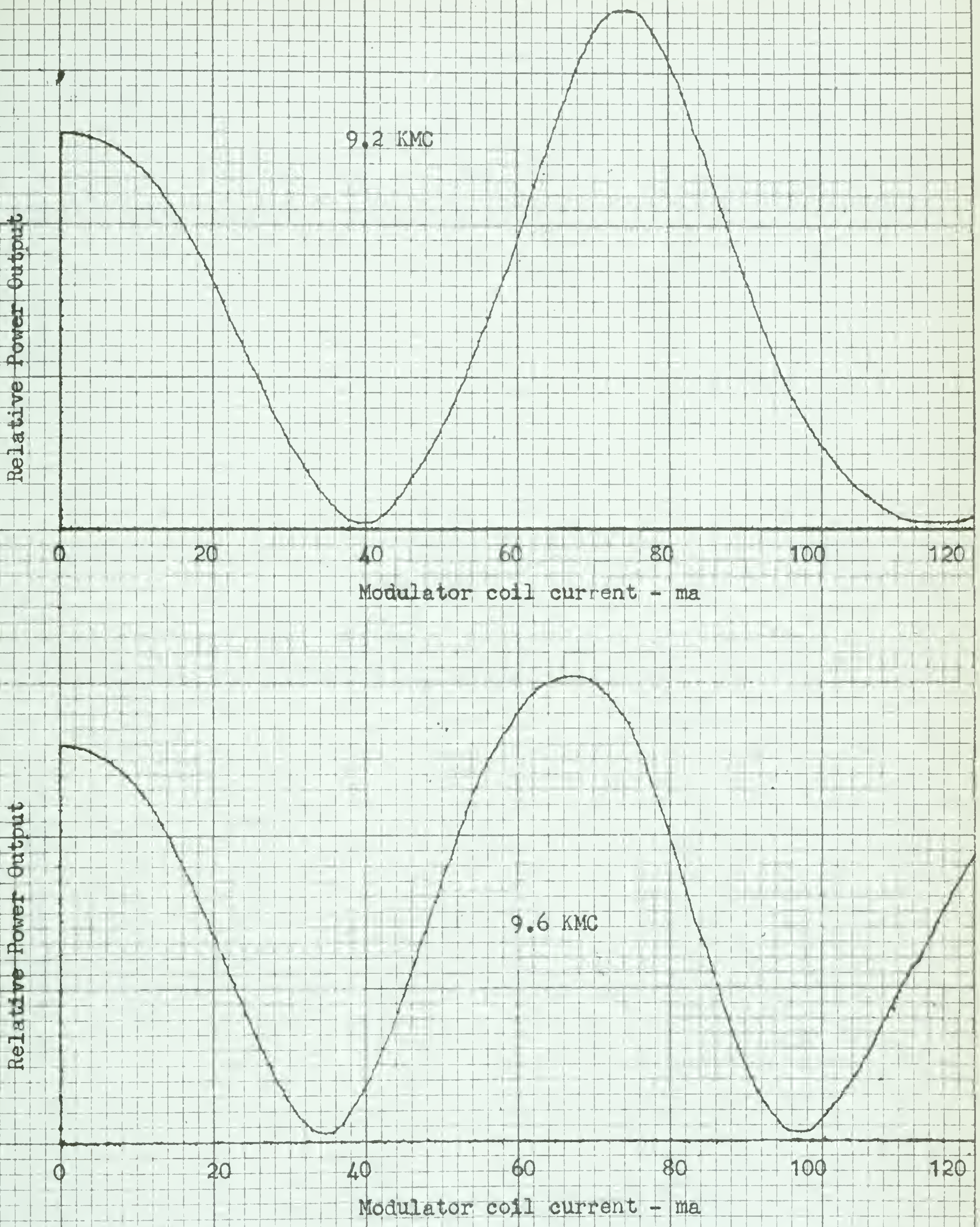

Fig.6-13. Transmission characteristics of the modulator as a function of applied current.

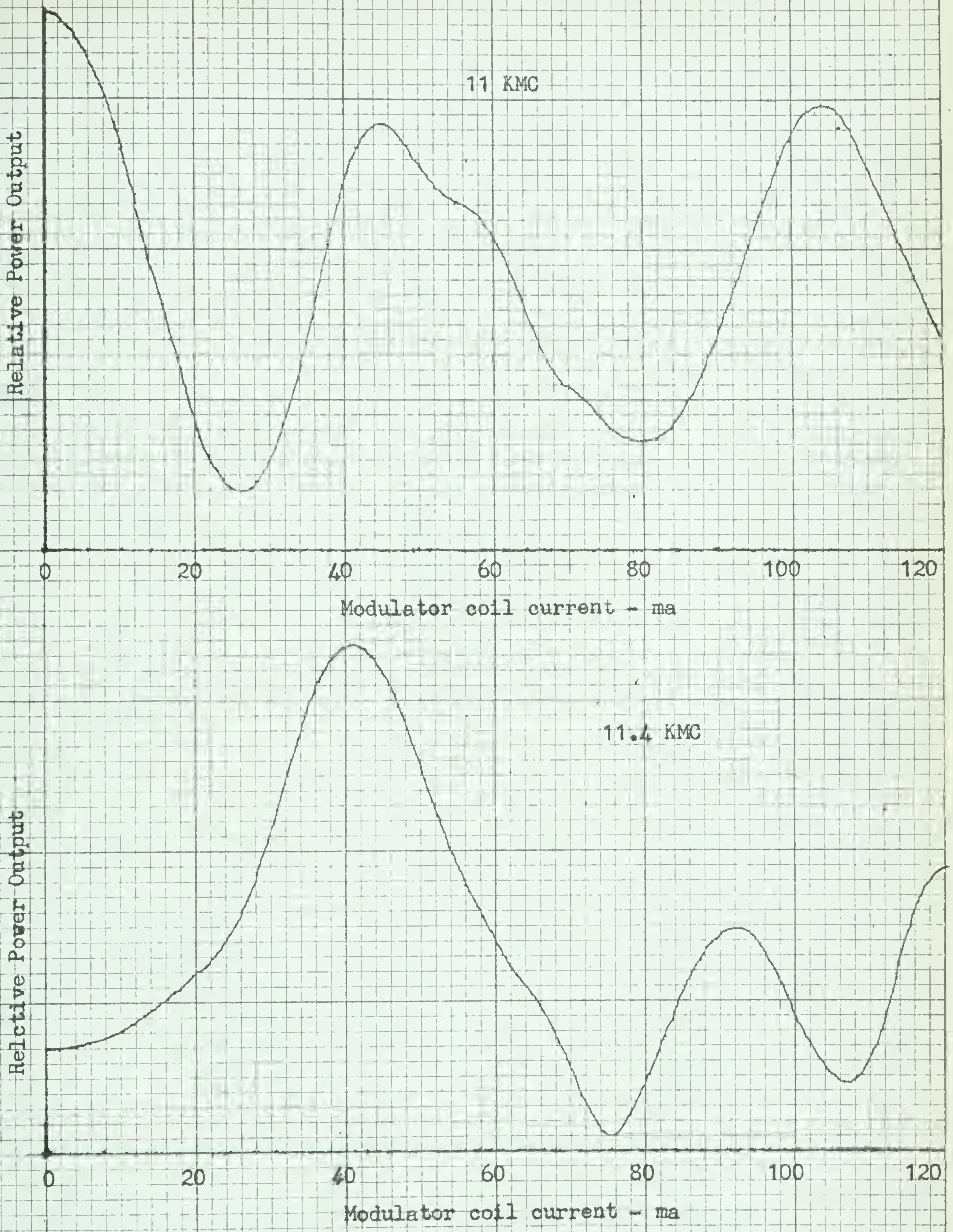

Fig.6-14. Transmission characteristics of the modulator as a function of applied current.

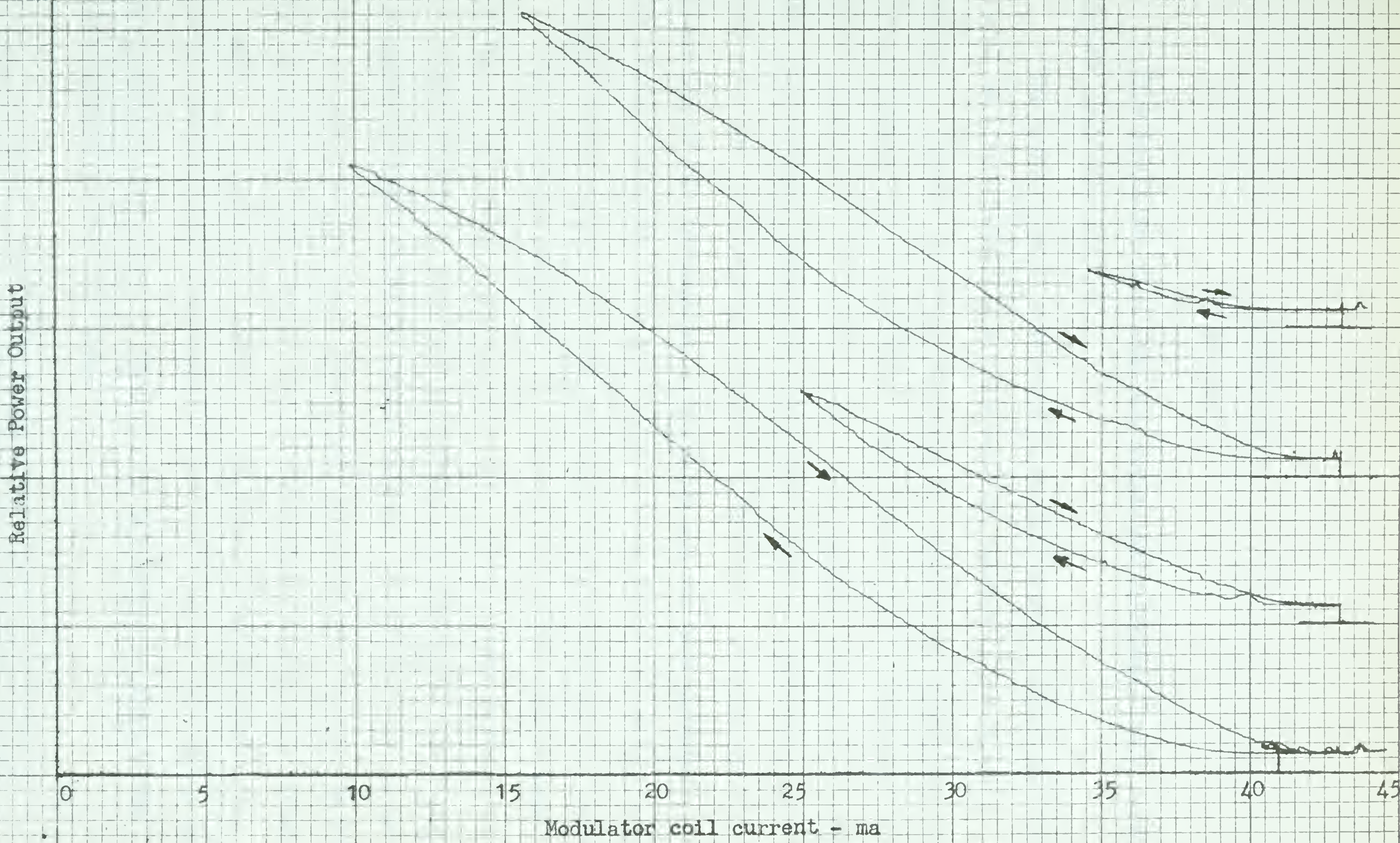

Fig.6-15. Static pulse modulation cycle showing hysteresis at 9 KMC

CHAPTER VII

CONCLUSION

This thesis has described the design and performance of a ferrite microwave amplitude modulator.

Only pulse signals were considered as modulating functions where one coil will satisfactorily perform both the modulating and biasing functions. However, for other waveforms the biasing and signalling functions should be assigned to two different coils, since for the praticular bias current required the 807 pentode does not necessarily operate in a linear region. The problems associated with general waveform modulation can be appreciated best by referring to Fig.6-18. Hysteresis effects and the cosine response law of the rectangular output guide are the main problems. To study general modulation some bias angle between 90° and 0° should be chosen and linear detectionwould be ideal to study modulation depths and distortion.

The microwave properties of the modulator require improvement depending on the intended application. The A-section data indicate that further improvements in both VSWR and losses are possible if the ferrite to waveguide diameter ratio is reduced further. The ferrite rod is not tapered in the present design. However,for improved VSWR the ferrite rod should be provided with tapers. This would,however, increase the required rod length to obtain the necessary rotations. Matched ferrite rods would also permit fuller utilization of Waldron's paper, but further data (static magnetization curve of ferrite rod) are needed to predict the current required for 90° rotation.

BIBLIOGRAPHY

1. C.D.Owen's, "A Survey of the Properties and Applications of Ferrites below Microwave Frquencies", Proceedings of the IRE, vol.44, October, 1956, pp. 1234-1248.

2. Legrand G. Van Uitert, " Dielectric Properties of and Conductivity in Ferrites", Proceedings of the IRE, vol.44, October, 1956, pp.1294-1303.

3. C.L.Hogan, " The Ferromagnetic Faraday Effect at Microwave Frequencies and its Application", Bell System Technical Journal, vol.31, January, 1952, pp. 1-31.

4. B.Lax and K.J. Button, " Microwave Ferrites and Ferrimagnetics", McGraw Hill Book Co., Inc., New York, 1962.

5. R.Plonsey and R.E. Collin, "Principles and Application of Electromagnetic Fields", McGraw Hill Book Co., Inc., New York, 1961, p.480.

6. G.T.Rado, "Theory of the Microwave Permeability Tensor and Faraday Effect in Nonsaturated Ferromagnetic Materials", Physical Review, vol.89, January, 1953, p.529.

7. R.A.Waldron, "Electromagnetic Wave Propagation in Cylindrical Waveguides containing Gyromagnetic Media", Journal of the British Institution of Radio Engineers, vol.18, 1958, pp. 597-612, pp.677-690, pp. 733-746.

8. G.S.Uebele, " High Speed Ferrite Microwave Switch", IRE National Convention Record pt.1, 1957, pp.227-234.

9. J.Millman and H.Taub, "Pulse and Digital Circuits", McGraw Hill Book Co., Inc., New York, 1956, p.41.

10. V.G.Welsby, "The Theory and Design of Inductance Coils", Macdonald and Co., London, 1950.

11. W.F. Gauster, " Some Basic Concepts for Magnet Coil Design", AIEE-Transaction, pt. Communications and Electronics, vol.79, January, 1961, pp.822-828.

12. "Radiotron Designers Handbook, 4th Edition, Radio Corporation of America, Harrison, N.J., Chapter 10.

13. H.J.Reich et al., "Microwave Theory and Techniques", D.Van Nostrand Company, Inc., Princeton, N.J., 1953, p.359.

14. E.L. Ginzton, "Microwave Measurements", McGraw Hil Book Co., Inc., New York, 1957, p.473.

B29831